Evaluation of Forest Road Scenarios Using Field Measurements and DHSVM Modelling of the South Fork of Caspar Creek

Final Report prepared for the California Department of Forestry and Fire Protection
Contract No. 8CA03637

September 22, 2020

Christopher G. Surfleet
Professor of Watershed Management and Hydrology
California Polytechnic State University
San Luis Obispo, CA 93407
csurflee@calpoy,edu

Contents

EXECUTIVE SUMMARY

This report presents an evaluation of forest road effects following the Phase III forest harvest (2017-2019) within the South Fork of Caspar Creek, Jackson Demonstration State Forest, California. A two-step approach was utilized: (1) road field measurements; and (2) use of the Distributed Hydrology Soil Vegetation Model (DHSVM) to examine road scenarios at the watershed scale. Storm runoff, turbidity, and suspended sediment measurements were collected for select forest roads in South Fork Caspar Creek during the winter of 2018-2019. Statistical relationships between road runoff, turbidity, and road dimensions to predict suspended sediment loads (SSL) were evaluated. DHSVM was calibrated and validated to two South Fork Caspar Creek gauging station records and road measurements for hydrologic years 2015-2019. DHSVM was used to extrapolate the measured road runoff and SSL relationships to evaluate the cumulative watershed effect. DHSVM also enabled different simulations of road network and drainage scenarios to evaluate the influence of different road practices. Quantification of uncertainty in DHSVM utilized a range of parameter inputs that provided a range of behavioral models, models that provide good fit to measured streamflow based on two likelihood function thresholds.

Statistical evaluation of road runoff, turbidity, and suspended sediment showed the best multiple linear regression model to predict Log10 suspended sediment load (SSL) from road runoff events was the event peak flow and cube root of maximum turbidity. Inclusion of cutslope cover or road surface type in the model explained significantly more variation in Log10 SSL relative to the model including only peak flow and cube root maximum turbidity. Both are measures of soil cover. Statistical evaluation using road dimensions and event precipitation to predict Log10 SSL, without runoff or turbidity, suggested the best model used road length times slope squared, road surface type, and cutslope area as explanatory variables. To predict storm peak flow from only road dimensions and precipitation suggested the best model used road length times slope squared and cutslope height as explanatory variables. Road dimensions of cutslope area and cutslope height had a negative relationship with SSL in the statistical analysis. In other words a greater cutslope area or height would reduce SSL. This can be explained by cutslope area being highly influenced by topographic position of the road.

DHSVM simulated streamflow provided good fit to the South Fork Caspar Creek streamflow time series of 2015-2019. However, the DHSVM model structure used did not simulate the threshold behavior of preferential flow that is common in Caspar Creek. Therefore, the accuracy of DHSVM simulations was lower for predictions of localized hillslope or hydrograph shape. The calibrated model was validated by showing reasonable fit to the Ziemer subwatershed, a much smaller tributary to South Fork Caspar Creek.

DHSVM simulations were run for two road networks and three different road drainage scenarios. The road networks were the 2018 road network with road placed near the top of

slopes away from watercourses to facilitate cable yarding, and the pre-1974 road network with a high density of roads adjacent to watercourses. The road scenarios simulated were:

1) No roads, for comparison of effects;
2) 2018 California Forest Practice Rules (CFPR) scenario which requires hydrologic disconnection of roads near watercourses;
3) Pre-2010 CFPR scenario without requirements of hydrologic disconnection; and
4) Pre-1973 CFPR scenario with little to no road drainage requirements.

There were low levels of suspended sediment contributions from the 2018 road network for both the 2018 and pre-2010 CFPR scenarios following forest harvest in the South Fork of Caspar Creek. The 2018 road network only had 3% of the total road length used in the harvest within 60 m (200 ft) of watercourses. There were much higher levels of suspended sediment contributions from the pre-1974 road network for the 2018, pre-2010, and pre-1973 CFPR scenarios following the forest harvest in the South Fork of Caspar Creek. The pre-1974 road network had, according to DHSVM model inputs, 58% of the total road length used in the harvest within 60 m (200 ft) of watercourses. However, previous studies have put this number at 75% of roads within 60 m (200 ft). The 2018 CFPR road scenario predicted lower sediment than the pre-2010 road rule scenario for both the 2018 and the pre-1974 road networks. The 2018 road rule scenario further decreased SSL in the pre-1974 road network to 22% - 36% of the pre-1973 CFPR scenario. However, even with this reduction in SSL contributions for the 2018 CFPR rule scenario SSL were approximately 10 times larger than the same scenario on the 2018 road network. The pre-1973 CFPR scenario with native surface roads near watercourses and infrequent to no road drainage structures contributed the highest levels of suspended sediment contributions of all scenarios.

The 2017-2019 forest harvest of South Fork Caspar Creek, reducing forest basal area by 42%, was predicted by DHSVM to increase storm peak flows by 1.5% to 11%. The Ziemer subwatershed, with a greater forest basal area reduction of 75%, was predicted by DHSVM to increase storm peak flows by 2.6% to 17.6%. The greater increase in peak flows in Ziemer is attributed to greater reduction of forest basal area. The 2018 road network with both 2018 and pre-2010 road scenarios only created a slight increase, < 2% difference, over the forest harvest associated peak flow increases for the South Fork and <1% in the Ziemer subwatershed. In contrast, the pre-1974 road network increased peak flows substantially above the forest harvest increases. The high end of the range of South Fork Caspar Creek peak flows were predicted by DHSVM to increase by 35% to 45% depending on road scenario. For the Ziemer subwatershed simulated peak flows, this range was increased to 40% to 87%. In both cases the pre-1973 CFPR scenario had that greatest effect, then the pre-2010 CFPR scenario, with the low end of the range from the 2018 CFPR scenario. These increases were for peak flows with less than a 4-year return interval. The results indicate that hydrological disconnection of road networks, as required by CFPRs, will mitigate increases in peak flows and suspended sediment. However road networks in close proximity to watercourses (in this study 58% or greater of total length within 60 m (200 ft), even with attempts at hydrologic disconnection, will still significantly contribute to cumulative watershed effects.

INTRODUCTION

The Caspar Creek Experimental Watersheds have provided foresters, land managers, researchers, and citizens with information that has influenced forest management in northwestern California since 1962 (Ziemer, 1998a; Cafferata and Reid, 2013; Dymond, 2015). The primary goal in establishing these experimental watersheds was to understand how harvesting timber could affect streamflow and suspended sediment concentrations (SSC). The first experiment, Phase I (1962 to 1985), was a classic paired watershed study undertaken before the implementation of the modern California Forest Practice Rules (CFPRs): roads were constructed in South Fork Caspar Creek (SFC) in 1967 and 1971 to 1973, and 60-70% of the timber volume was selectively harvested by tractor yarding from 1971 to 1973 (Figure 1). North Fork Caspar Creek served as a control (Rice et al., 1979). The second experiment, Phase II (1985 to present), studied cumulative watershed effects using California Forest Practice Rules not in existence in the first experiment. Watercourse and lake protection zones (WLPZs), limits on clearcut size, adjacent harvest restrictions, and road placement and drainage requirements were some of the improvements in forest practices investigated in the North Fork of Caspar Creek (Ziemer, 1998a; Lewis et al., 2001). In South Fork of Caspar Creek, streamflow and SSC measurements began in 2000 for a network of subwatersheds in anticipation of a third experiment, Phase III that would investigate the impact of harvesting under updated CFPRs (Dymond, 2015; Wagenbrenner, 2018).

Phase III Experiment

The third experiment at Caspar Creek was designed to expand upon the findings of the first two experiments by investigating hydrologic, geomorphic, and ecological processes in coast redwood forests at the tree, plot, hillslope, sub-basin, and catchment scales (Dymond, 2015). This third experiment is studying the effect of stand density reduction (i.e. reducing the quantity of trees) on watershed processes and characteristics on sites while utilizing the current CFPRs. In the original study plan, several goals were put forth for the Phase III experiments (Wagenbrenner, 2018). This report presents the efforts to address goal 5, calibrate the Distributed-Hydrology-Soil-Vegetation Model (DHSVM) (Wigmosta et al., 1994) for the Caspar Creek Experimental Watersheds in order to simulate the effects of different silvicultural and road building practices on streamflow and sediment. It complements the DHSVM modeling study completed for the South Fork modeling changes in stream temperature with varying CFPR requirements by Ridgeway (2019).

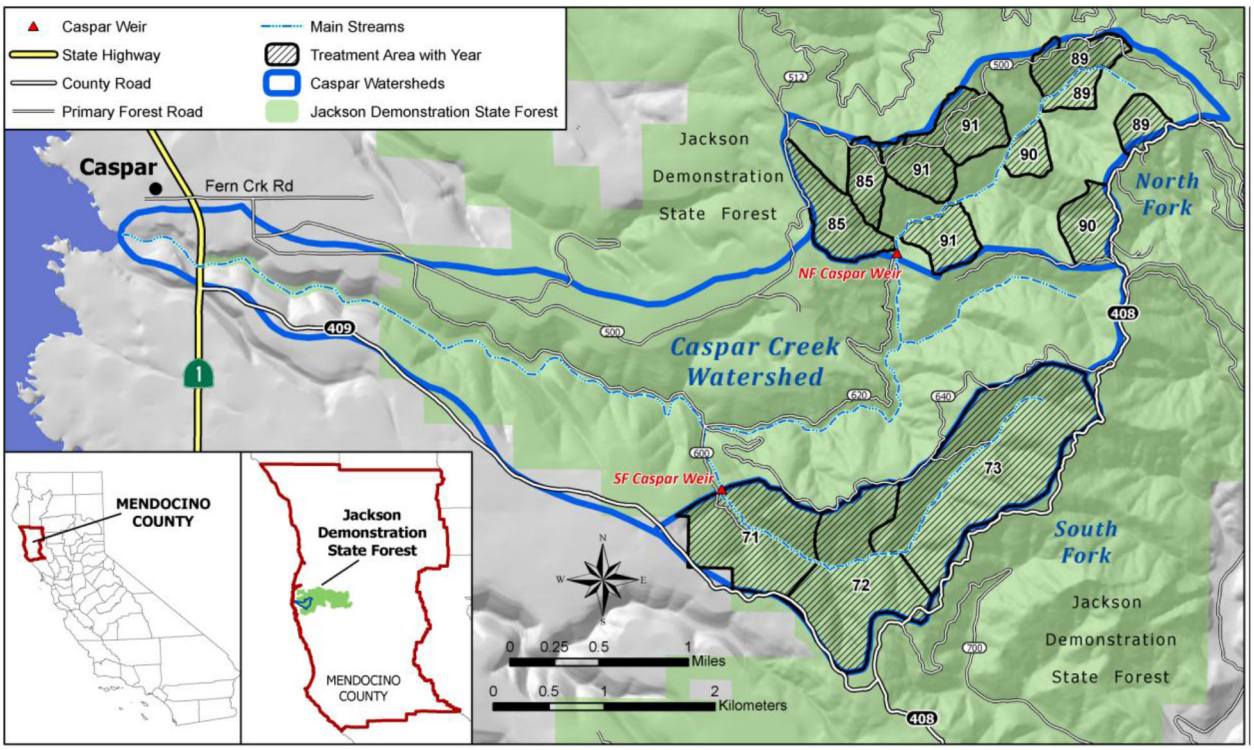

Figure 1. The Caspar Creek Experimental Watersheds are located on the north coast of California. Numbers indicate the year in which timber harvest began for Caspar Creek Phase I and II. From Cafferata and Reid (2013).

California Forest Practice Rules – New Road Regulations

New forest practice rules were implemented in California beginning in January 2010 requiring improved practices for watersheds with listed anadromous salmonids; Anadromous Salmonid Protection (ASP) rule package. These new rules required road hydrologic disconnection and a stable operating surface for logging roads. Statewide requirements for hydrologic disconnection and suggested spacing for rolling dips and cross drain culverts, as well as updated road construction, maintenance, and management regulations, were implemented in January 2015. As defined in 14 CCR § 895.1, hydrologic disconnection means the removal of direct routes of drainage or overland flow of road runoff to a watercourse or lake (CAL FIRE, 2018). The goal of hydrologic disconnection is to minimize sediment associated with road runoff from being delivered to a watercourse (Weaver et al., 2015). Hydrological disconnection of roads requires frequent road drainage to (1) reduce the volume of road-generated overland flow, (2) promote infiltration of road overland flow, and (3) direct road overland flow away from watercourses. By relieving road runoff from short road segments less runoff volume and the associated sediment generated from the road is concentrated on forest soils or delivered to watercourses. Hydrologic disconnection is focused on roads in close proximity to watercourses (CAL FIRE, 2018, Technical Rule Addendum No. 5).

Goal and Objectives

The goal of this study is to use DHSVM paired with road runoff, turbidity, and suspended sediment measurements to estimate the surface erosion and hydrologic effects from forest roads in the South Fork of Caspar Creek. Specific objectives to meet this goal are:

(1) Measure road runoff and sediment from select road points following the Phase III experiment forest harvest (2017-2019).

(2) Evaluate physical road dimensions, turbidity, and road runoff for prediction of road suspended sediment yield.

(3) Calibrate DHSVM, within a model uncertainty assessment, to streamflow and road runoff for the South Fork of Caspar Creek.

(4) Pair DHSVM simulated streamflow and road runoff to suspended sediment loads.

(5) Simulate the effect on peak flows and suspended sediment for different road management scenarios associated with changes in the California Forest Practice Rules.

METHODS

OVERVIEW OF RESEARCH APPROACH

To meet the goal and objectives of the research a two-step approach of (1) road field measurements, and (2) DHSVM road runoff and streamflow simulations was used. Storm runoff, turbidity, and suspended sediment measurements were collected for select forest roads in South Fork Caspar Creek associated with the Phase III experiment forest harvest. The roads were winterized by installing waterbreaks, stopping all heavy equipment use on roads, and blocking use on temporary roads in fall of 2018 following the forest harvest. The winterization of roads was done using road practices that attempt to provide hydrologic disconnection of the roads, as required by the CFPRs (CAL FIRE, 2018). The Distributed Hydrology Soil Vegetation Model (DHSVM) was calibrated to two South Fork Caspar Creek gauging station records and road measurements from the winter of 2018-2019. DHSVM was used to extrapolate the measured road runoff and SSC relationships to evaluate the cumulative watershed effect. DHSVM also enabled different simulations of road drainage and road placement scenarios to evaluate the influence of different potential road practices.

STUDY AREA

The study location is the South Fork of Caspar Creek within the Caspar Creek Experimental Watersheds on the Jackson Demonstration State Forest (JDSF), California, USA (Figure 1). JDSF is located in the northern part of the California Coast Ranges geomorphic province. The South Fork Caspar Creek watershed encompasses 417 ha, with the outlet located at 39.313^{o} N, -123.753^{o} W (Figure 2).

South Fork Caspar Creek has a Mediterranean climate; the fall and winter seasons are characterized by a westerly flow of moist air that typically results in low-intensity rainfall and prolonged cloudy periods with only rare occurrences of snow (Henry, 1998). The average annual precipitation for the watershed is 1170 mm, with nearly 50% resulting in streamflow, and

the residual lost either to evapotranspiration or groundwater (Carr et al., 2014). The geology at Caspar Creek consists of Franciscan sandstone bedrock overlain by 1 to 4 m of highly permeable loam soils (Carr et al., 2014; Henry, 1998). The dominant soil sub-groups are Mollic hapludalf, Ultic haludalf, and Typic hapluhumult (Dymond, 2015). South Fork Caspar Creek is a forested watershed with primarily second and third growth coast redwood (*Sequoia sempervirens*), Douglas-fir (*Pseudotsuga menziesii*), grand fir (*Abies grandis*), and tanoak (*Notholithocarpus densiflorus*). There are minor components of western hemlock (*Tsuga heterophylla*), red alder (*Alnus rubra*), and scattered bishop pine (*pinus muricata*) (Henry, 1998).

South Fork Caspar Creek Hydrologic Measurement and Forest Harvest in the Phase III Experiment

The Phase III experiment had a total of eleven gaging stations installed to monitor streamflow and suspended sediment concentrations of subwatersheds in South Fork Caspar in 2000 (Dymond, 2015). A portion of the mid-slope spur road was abandoned in 2011, and approximately three miles (4.6 km) of the streamside roads built in 1967 were decommissioned in 1998 (Keppeler et al., 2007; Keppeler 2012). The road network for South Fork Caspar Creek in 2019 is shown in Figure 2. Note that not all roads shown were associated with the forest harvest. However all roads, even if not used in the harvesting, within the watershed were evaluated due to potential hydrologic or suspended sediment effects.

The Phase III experiment implemented varying basal area reductions in eight subwatersheds, ranging from 0% to 75% (Table 1). Stand density reduction across the South Fork Caspar Creek was approximately 42%. The silviculture used to implement the stand density reduction rates was generally single tree selection harvests used toward uneven-aged management. The exception was watersheds with higher density reduction targets for the actively managed portion of the Ogilvie and Ziemer subwatersheds (Figure 3). In these areas fewer trees were retained by using CFPR variable retention method. The basal area reduction targets by subwatershed are shown in Table 1.

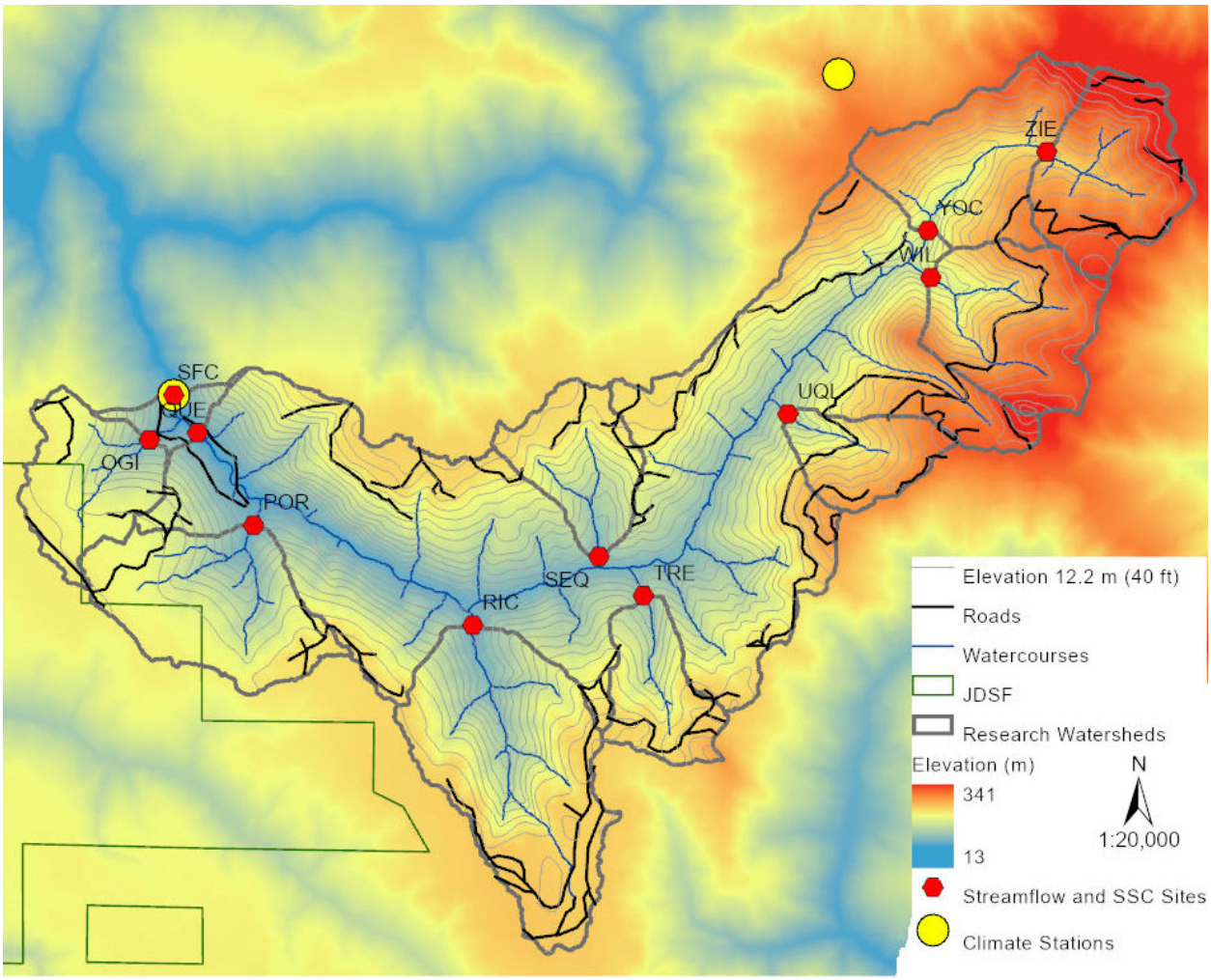

Figure 2. South Fork Caspar Creek research watersheds and subwatersheds with gauging station locations. The road network within the South Fork in 2018 and the climate station locations adjacent to the South Fork are shown. Gauge abbreviations are defined in Table 1.

Table 1. Forest harvest basal area reduction for the subwatersheds in SFC. Pre-treatment basal area provided by Kirk O'Dwyer and Lynn Webb, Jackson Demonstration State Forest.

Watershed Name	Gauge ID	Area (ha)	Pre-treatment Basal Area (m^2 ha^{-1})	Reduction (%)
South Fork Caspar Creek	SFC	417	87.9	42%
Ogilvie	OGI	18	79.4	45%
Porter	POR	32	78	25%
Richards	RIC	49	87.1	-
Sequoyah	SEQ	17	94.4	65%
Treat	TRE	14	99.1	35%
Uqlidisi	UQL	13	76.6	55%
Williams	WIL	26	99.1	-
Yocom	YOC	53	90.39	43%*
Ziemer	ZIE	25	86.5	75%

*The Yocum watershed encompasses Ziemer, but no additional harvesting occurred downstream of the ZIE gauge.

Figure 3. Ziemer subwatershed in 2018 during cable yarding (left) and after Phase III timber harvesting (right), with a watershed wide stand density reduction of 75% through a variable retention harvest (photo credit (right) Ryan McGrath, June 2018).

ROAD RUNOFF PILOT STUDY

Road Runoff Measurement Flumes

Road hydrologic measurements were collected in a circular flume as described in Samani and Herrera (1996). This type of flume is a low-cost water measuring device made with PVC pipe. All parts of the flume were purchased at a plumbing or hardware store and built by hand. The riser in the circular flume had holes drilled to allow water to enter and act as a stilling well to allow use of electronic stage recording instruments (capacitance rods or pressure transducers) or crest-stage gages (Figure 4). Prior to installing flumes in the field, the flume calibration, or published rating curve (Samani and Herrera, 1996), was tested by running water at varying flow levels through the flumes. A graduated cylinder and stopwatch measured the flow. In anticipation of field installations on road segments with differing slopes, we altered the flume slope in the test from 3% to 5%. We found differences from the published rating curve and created our own depth to discharge relationship (Figure 5). We believe the difference from our calibration to the published calibration is due to difference in flume slopes. The measurement of stage by a depth recorder within the riser may also be associated with the different calibration. The published calibration is based on measurements made outside the riser, on the side directed toward the incoming flow.

Figure 4. Cal Poly student Grace Goldrich-Middaugh running water into the circular flume to test the stage to water flow relationship. The PVC riser in the center creates a hydraulic jump to allow measurement of stage for flow correlations. The riser also acts as the stilling well for the flume. The cable exiting the riser is the interface cable for a pressure transducer making stage measurements.

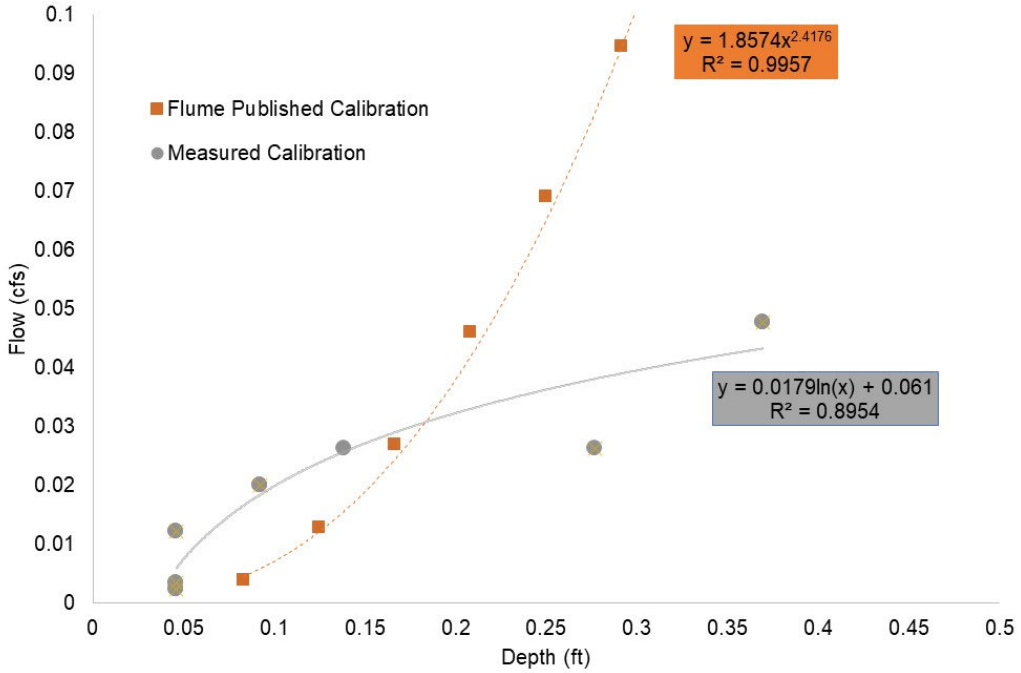

Figure 5. Depth to flow rating curve test for a circular flume. We used the measured calibration for this study, since the published rating curve over-predicted flow. We speculate that the location of stage measurement in the flume and putting the flume on a range of sloped positions, as were encountered for road applications, are the reasons for the difference from the published calibration curve.

Road Pilot Study Winter 2017 to 2019

During winter 2017-2018 a pilot study was conducted at Caspar Creek to test the ability of small homemade flumes and inexpensive depth recorders to measure road runoff. A total of 10 handmade road flumes were installed in road ditches or the outlets of waterbreaks on varying road segments in the South and North Forks of Caspar Creek in December 2017. Of the 10 flumes, six were installed with inexpensive continuous depth recorders by Onset and four with crest-stage gauges (using cork). JDSF Forester Kirk O'Dwyer and United States Forest Service Pacific Southwest Research Station (USFS PSW) staff checked the flumes periodically. Throughout the winter debris and sediment needed to be cleaned from the flumes. Occasionally a flume was found completely plugged. We learned from this pilot that the road runoff depth and peak flow depth by crest-stage gauge appeared to be effectively measured by the homemade flumes (Figure 6). However, the flumes needed constant attention throughout the winter to ensure they were not plugging with sediment and debris. The Onset depth recorders required correction by atmospheric pressure. Depending on the proximity and timing of the atmospheric pressure, the Onset pressure transducers had high variability around the actual depth.

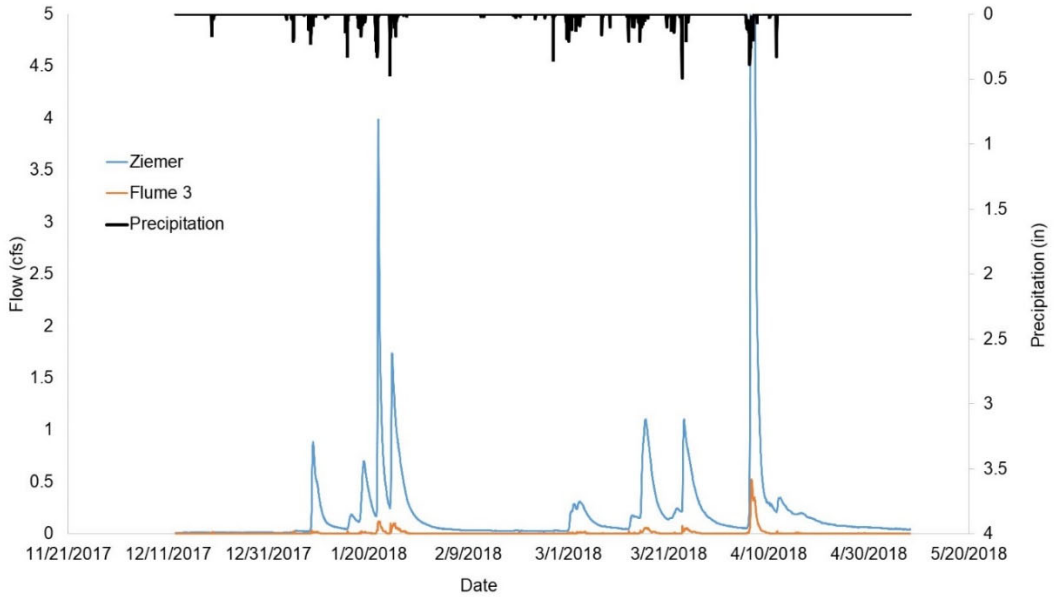

Figure 6. Comparison of a road flume runoff measurement and ZIE streamflow, December 2017 to April, 2018, during the road runoff pilot study. Road runoff generally corresponded to stream storm runoff in a flume with road runoff continuous measurement and no plugging.

RUNOFF, PEAK FLOWS, TURBIDITY, AND SUSPENDED SEDIMENT MEASUREMENT FROM ROADS FOLLOWING FOREST HARVEST

The field measurements of road segments occurred the winter following the 2018 South Fork Caspar Creek timber harvest. Data collection from the road segments occurred from November 20, 2018 to April 15, 2019. Several different types of data collection occurred on the forest roads with varying timing, described below.

Road Measurement Selection

Road segments were selected within and adjacent to the South Fork Caspar Creek watershed for evaluation. There were 16 road points selected, attempting to capture varying road lengths, slope position (ridge, midslope, lower slope, swale, spur), road surface (native, rocked), and amount of log truck traffic. Another criteria for measurement was the ability to install a small circular flume for runoff or peak flow measurement (road flumes). Road flume performance was optimal when they were installed in road inside ditches, which were not a common feature in the South Fork Caspar Creek watershed (Figure 6), since the new road segments were outsloped with rolling dips when the road gradient was $\leq$7%.[1] Road flumes could also be installed at the

[1] The timber sale contract specified that roads were to be constructed with a 2-5% outslope and without a berm or inside ditch. The road surface was to be insloped or bermed only where needed to direct water to a drainage facility or away from a sensitive area. Where the road grade was 7% or less, permanent and seasonal roads were to have rolling dips incorporated into their running surface during their construction.

outlet of rolling dips or waterbreaks, provided the road discharge was completely directed toward the flume. Many road segments, however, lacked these features. The road point selection also attempted to capture a spatial balance of sites across the watershed area (Figure 7). The road network associated with the Phase III experiment was primarily limited to ridge top spur roads. Due to the low density of existing roads in the experimental watershed and the need to capture varying road dimensions or conditions, a randomized sampling approach was not utilized.

Figure 7. Homemade road flume placed in a road ditch of the South Fork of Caspar Creek. Concrete mortar and sand bags at the inlet ensured all ditch flow entered the flume. Some installations used clay or weathered sandstone to seal the flume inlet instead of concrete.

Road Measurement Locations and Dimensions

The 16 road sites (numbered 1 to 17; number 2 was excluded due to damage) were studied during the winter of 2018 - 2019 within or adjacent to the South Fork Caspar Creek (Figure 8; Table 2). Of these 16 road segments, six sites had continuous turbidity, suspended sediment, and discharge (RTS) data collected during precipitation events. The remaining ten road segments only measured peak discharge during precipitation events with crest-stage gauges. There were two additional road sites established to evaluate road turbidity influences above and below a Class I and Class II watercourse crossing (sites CI, CII; Figure 8).

Road dimensions of length and width of road tread or ditch were determined during precipitation events. Visual evidence of the portion of the roads that contribute overland flow were used to determine these dimensions.

Table 2. Road segments and their dimensions used for measurement of peak discharge (crest-stage gauges) or runoff, turbidity, and suspended sediment (RTS) for road segments in or adjacent to South Fork Caspar. Road measurement sites for one Class I watercourse crossing (CI) and one Class II watercourse crossing (CII) with above and below turbidity and discharge measurements are included. There was not a site ID number 2; site 6 was adjacent to CII crossing.

Site ID	Road Length m (ft)	Road Width m (ft)	Ditch Width m (ft)	Ditch Depth m (ft)	Cutslope Height m (ft)	Slope (%)	Cutslope Cover (%)	Surface Type	Type/Comment
1	19.8 (65)	4 (13)	-	-	3 (10)	14	70	native	crest, no ditch
3	92.1 (302)	2.7 (9)	1.5 (5)	0.6 (2)	1.2 (4)	10	60	rocked	crest
4	39.2 (129)	2.4 (8)	1.8 (6)	0.6 (2)	3.4 (11)	10	80	rocked	crest
5	12.2 (40)	2.7 (9)	-	-	1.5 (5)	10	35	native	no ditch
7	79.3 (260)	-	1.8 (6)	0.6 (2)	9.1 (30)	10	100	rocked	RTS, ditch only
8	61 (200)	3 (10)	1.8 (6)	0.9 (3)	2.1 (7)	6	100	rocked	crest
9	41.2 (135)	-	1.8 (6)	0.6 (2)	0.6 (2)	5	95	rocked	RTS, ditch only
10	113 (370)	1.5 (5)	1.5 (5)	0.3 (1)	7.6 (25)	1	98	rocked	crest
11	43.3 (142)	3 (10)	1.5 (5)	0.6 (2)	1.2 (4)	2	90	rocked	RTS
12	38.1 (125)	5.2 (17)	-	-	2.1 (7)	11	75	native	crest, no ditch
13	94.5 (310)	4.3 (14)	-	-	0.9 (3)	8	50	native	crest, no ditch
14	27.4 (90)	4.6 (15)	-	-	2.1 (7)	8	40	native	crest, no ditch
15	61 (200)	6.6 (22)	-	-	1.5 (4.9)	14	20	native	RTS, no ditch
16	39 (128)	6 (20)	-	-	0.4 (1.3)	16	15	native	RTS, no ditch
17	26 (85)	7 (23)	-	-	0.2 (0.7)	15	20	rocked	RTS, no ditch
Above and below watercourse crossing									
CII 6	12.2 (40)	-	1.8 (6)	0.6 (2)	0.9 (3)	14	90	rocked	Class II Road 640 Site 6 crest
CI East	79.3 (260)	-	1.8 (6)	0.6 (2)	9.1 (30)	10	20	rocked	Road 620 east side, ditch only
CI West	54.9 (180)	4.9 (16)	1.8 (6)	0.6 (2)	n/a	2	100	rocked	Road 620 west side

Road Instruments and Procedures

Road Runoff, Turbidity, and Suspended Sediment Sites (RTS)

The six instrumented road flume sites were equipped with a pressure transducer, turbidity meter, and pump sampler (Figures 9 and 10). The turbidity meters used were OBS-3 models (Campbell Scientific, Logan, Utah). The pressure transducers were a mix of Druck models 1830 and 950 (Baker Hughes Digital Solutions). The pressure transducer and turbidity probe interfaced to a Campbell Scientific CR510 datalogger. The pump sampler was a Global Water WS700 composite sampler (Xylem Analytics, Letchford, UK), with a 10 liter (2.5 gallons) sample capacity. The USFS PSW provided dataloggers, turbidity probes, and pressure transducers for this study.

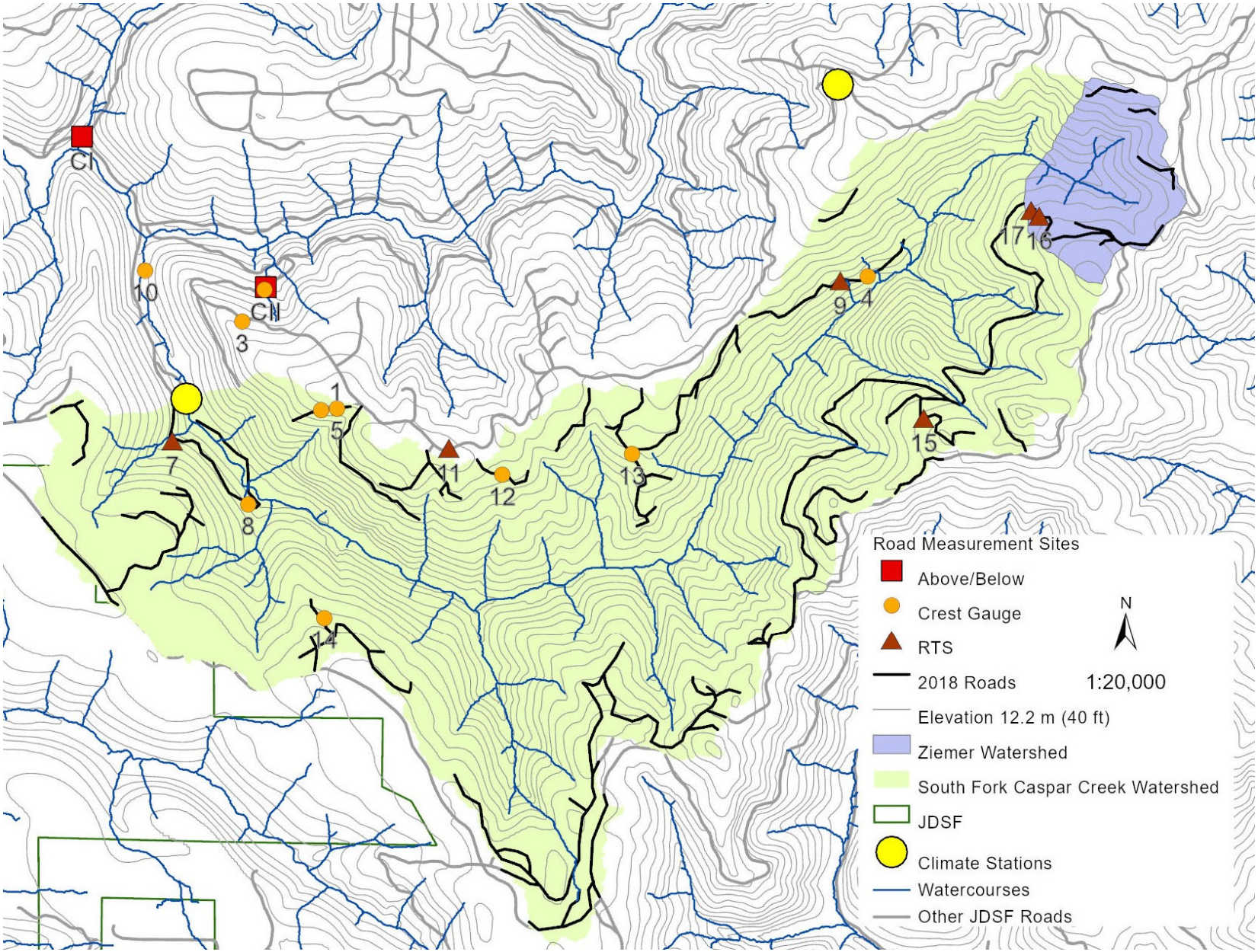

Figure 8. Locations of road study sites in or adjacent to South Fork Caspar Creek. Road RTS sites had runoff, turbidity, and suspended sediment measurements during precipitation events. Road crest-stage gauge sites only measured peak discharge for precipitation events. Above and below turbidity sites at watercourse crossings were sites CI and CII (see Table 2 for details on the road segments).

After several iterations, an alternative design was created for the suspended sediment and turbidity measurements. This alternate design was used on road sites 15 and 16, roads with high road runoff and native surfaces. With the alternative design the reservoir was placed on a slight angle, approximately 15%, which created approximately a 2-inch depth of water for turbidity and suspended sediment measurements. A hole was placed at the bottom of the reservoir, and the hole was rotated to a level consistent with the depth required for turbidity readings in the reservoir. The slight angle and hole in the reservoir created a situation where sediment settled below a water depth needed for turbidity measurements (Figure 10).[2]

At the start of precipitation events, the instruments were turned on by connection to a 12-volt battery. All precipitation events (storms) had measurements of stage and turbidity at 10-minute intervals. Select storms had water samples from road runoff collected. The pump sampler was turned on and samples of 100 ml were taken every hour. During precipitation events flumes were checked for blockage, sediment deposition, and instrument malfunctions.

At the end of the precipitation event the composite sample from the storm was collected. This composite sample was assumed to be representative of the average sediment concentration throughout the runoff event. The sample container was mixed and a 1-liter bottle was filled from the composite sample. The 1-liter bottle was put on ice, then transported to Alpha Analytical Labs in Ukiah, California. The samples were filtered and total solid (mineral and organic materials) concentration (mg/l) was provided. Suspended sediment load from the precipitation events was calculated by multiplying the total solids concentration by the discharge at the road flume, then summed by time interval for the storm.

Crest-Stage Gauge Sites

There were 10 road sites where only crest-stage gauges were installed at the road flumes (Figure 8). Cork and a wooden stick were placed in the riser of the road flume. The elevation of the floor of the water flow section of the flume was determined and marked on the stick. During road runoff events the water level and cork would rise. When the runoff event receded, the cork remained on the stick at the highest water level. This peak discharge stage was determined by measuring the change in elevation of the cork compared to the flume bottom. Flumes were cleaned between storm events. The stick had cork removed from the previous event and the riser was replenished with cork if needed. The remote location of several of the road flumes prohibited measurement of the peak discharge for every storm event. Knowledge of the peak discharge from roads provided data useful for calibrating the road runoff modelling with DHSVM.

[2] Many thanks to Samasoni Matagi, Hydrologic Technician working on this study, who created this solution to our sampling challenges.

Figure 9. Road site 15 with the initial suspended sediment and turbidity measurement design. The PVC pipe to the left had a T-junction with a reservoir below to allow sufficient depth and mixing of water for sampling. On native surface roads, this design failed due to the reservoir filling with sediment. This design worked on rocked roads with low sediment contributions. The pump sampler is the grey box to the left; the data logger is in the plastic tote.

Figure 10. Alternative turbidity and suspended sediment measurement design for high sediment production roads. The reservoir below the road flume is on an angle to pond water and sediment. A drain hole at the end of the reservoir is set at a level that allowed water to pond above the sediment deposition in the reservoir to a depth sufficient for turbidity measurement of the water.

Turbidity Differences Above and Below a Class I and Class II Watercourse – Case Study

Continuous streamflow and turbidity were measured above and below two watercourse crossings within the Caspar Creek watershed, adjacent to South Fork Caspar Creek (Figure 8: CI and CII sites). The two sites were a case study attempting to quantify the difference in turbidity in watercourse storm runoff from a road crossing. One crossing was at a Class I watercourse (CI) over Blue Gum Creek on JDSF Road 600. The other crossing was at a Class II watercourse (CII) on Road 640 (see Table 2 for road dimensions). At both watercourse crossings, a standpipe was installed at the inlet of the watercourse crossing culvert (Figure 11). A pressure transducer was placed in the standpipe to record stream stage. At both crossings turbidity probes were placed in well mixed sections of the watercourse with enough depth and volume for the turbidity measurement. A turbidity probe was placed upstream and downstream of the crossing. A third crossing, at a Class III watercourse, was prepared for measurement but did not flow water during the winter of 2018 to 2019.

The instruments at the Class I watercourse crossing were installed in early January 2019 and removed March 5, 2019. Several select storm events were captured at this location. The instruments at the Class II watercourse crossing were installed in mid-January 2019 and removed March 5, 2019. The smaller and steeper watercourse at the Class II crossing presented difficulties finding a good placement for the turbidity probes. Select storm events were captured in February 2019 up to March 5, 2019. The above and below crossing sites were not given top priority for maintenance during storm events.

Figure 11. Left image: Standpipe for stage measurement at the inlet of the culvert on the Class I watercourse crossing; Blue Gum Creek JDSF road 600. Right image: Turbidity probe installed on the upstream side of the Class I watercourse crossing. The container on the bank contains the probe's data logger.

Data Filtering and Correction

The turbidity and stage measurements for the six road sites with sediment turbidity data and the two watercourse crossings utilized equipment from the USFS PSW Caspar Creek Watershed Experiment. The Campbell Scientific data loggers were programed for turbidity threshold sampling (TTS) used for the monitoring stations throughout the South and North Fork of Caspar Creek (Lewis and Eads 2009). This study did not use TTS, but data were collected within the TTS program, minus the pump sampler. A program developed by the USFS PSW titled TTS Adjuster was used to make corrections to turbidity and stage measurements within the TTS framework. Adjustments were made for anomalous turbidity spikes, corrections for offset in stage measurement, and removing or making an interpretation for time periods with known problems indicated in the field notes.

Data Collected by Site

Table 3 summarizes the data output for each site and storm for November 2018 to April 2019. Note that storms for the road study were any precipitation event which created road runoff. This is a lower threshold for storms as defined for streamflow and TTS stations in South Fork Caspar. We identified 28 storms from November 2018 to April 2019, including 7 storms identified at the SFC weir for the same period (Table 4).

Table 3. Output data collected for each road site during the winter of 2018 to 2019. Storm dates and time by storm number are found in Table 4. RTS = runoff volume, peak flow, turbidity, sediment; P = peak flow only, RT = runoff volume, peak flow, turbidity. Road sites were not visited for storms 23-27.

Storm No.	Road Site															
	1	3	4	5	6	7	8	9	10	11	12	13	14	15	16	17
1										RTS			P	RTS	RTS	RTS
2										RTS				RTS	RTS	RTS
3										RTS				RTS	RTS	RTS
4										RTS				RTS	RTS	RTS
5														RTS	RTS	RT
6														RTS	RTS	RTS
7						RT		RT		RT				RT	RT	RT
8	P	P		P	P	RT	P	RT		RTS				RTS	RTS	RTS
9						RTS		RTS		RTS				RTS	RTS	RTS
10	P		P	P	P	RT	P	RT	P	RT		P		RT	RT	RT
11	P	P	P	P	P	RT	P	RT	P	RT				RT	RT	RT
12		P	P		P	RTS	P	RTS	P	RTS				RTS	RTS	RTS
13	P		P	P		RTS	P	RTS	P	RTS	P	P	P	RTS	RTS	RTS
14						RTS				RTS				RTS	RTS	RTS
15	P	P	P	P	P	RTS	P		P	RTS	P	P	P	RTS	RTS	RTS
16	P	P	P	P	P	RT	P	RT	P	RT	P	P	P	RTS	RT	RT
17	P	P	P	P	P	RT	P	RT	P	RT	P	P		RTS	RT	RT
18	P	P	P	P	P	RTS	P	RTS	P	RTS	P	P	P	RTS	RTS	RTS
19						RT		RT		RT				RT	RT	RT
20						RT		RT		RT				RT	RT	RT
21	P		P	P	P	RT	P	RT	P	RT	P	P	P	RT	RT	RT
22	P				P	P	P	P	P	RT				RT	RT	RT
28	P	P	P	P	P	P	P	P	P	P	P	P	P	P	P	P

Table 4. Storm start and stop times for data analysis. Storm start and stops were interpreted based on interpretation of hydrographs from the SFC weir streamflow with the exception for events with sediment data collected. When sediment data were collected the time sampling stopped defined the storm, which in a few cases spanned multiple precipitation events with only short breaks between. *Storms with * indicates a storm with overlap with storms events from the SFC weir; road measurements did not encompass the entire storm event time period recorded at SFC.*

Storm No.	Start Time	Stop Time		Storm No.	Start Time	Stop Time
1	11/21/2018 3:10	11/24/2018 9:50		15*	1/18/2019 5:40	1/21/2019 19:40
2	11/27/2018 4:50	11/28/2018 3:10		16	2/1/2019 0:30	2/3/2019 0:00
3	11/28/2018 20:40	11/30/2018 0:40		17	2/3/2019 8:50	2/5/2019 19:20
4	11/30/2018 10:00	12/2/2018 11:10		18*	2/8/2019 14:20	2/17/2019 19:00
5	12/4/2018 16:40	12/5/2018 19:00		19	2/20/2019 2:50	2/20/2019 12:20
6	12/9/2018 15:40	12/10/2018 14:10		20*	2/24/2019 2:50	2/28/2019 13:20
7	12/14/2018 8:40	12/15/2018 3:30		21*	3/1/2019 19:30	3/4/2019 11:30
8	12/15/2018 11:00	12/17/2018 15:40		22	3/5/2019 9:20	3/8/2019 2:20
9	12/18/2018 5:50	12/19/2018 13:30		23	3/9/2019 12:20	3/13/2019 21:10
10	12/20/2018 0:50	12/22/2018 0:20		24	3/20/2019 6:50	3/23/2019 23:00
11	12/23/2018 7:50	12/26/2018 15:10		25	3/25/2019 3:00	3/26/2019 20:00
12	1/5/2019 4:30	1/7/2019 23:30		26	3/28/2019 11:30	4/1/2019 1:20
13	1/8/2019 6:40	1/11/2019 17:50		27*	4/5/2019 2:00	4/7/2019 3:10
14*	1/15/2019 2:20	1/17/2019 12:00		28*	4/8/2019 5:00	4/10/2019 14:00

Statistical Evaluation of Road Measurements

Overview

Ordinary least squares multiple linear regression (MLR) was used to evaluate physical road dimensions, turbidity, and road runoff for prediction of storm suspended sediment load (SSL) at the six road flume sites monitored during winter 2018 - 2019. The road sites with continuous runoff, turbidity, and suspended sediment (RTS) data collected during road runoff events were flumes 7, 9, 11, 15, 16, and 17. Table 5 summarizes the explanatory variables used in the MLR model selection process to predict SSL, including specific physical road parameters. Storm volume determined from road runoff measurements was not used as an explanatory variable in the model selection process because this variable was used in the calculation of SSL and thus is naturally correlated with the response.

All statistical analyses of road measurements were performed using Minitab Statistical Software (version 18.1). Best subsets, forward selection, and backward elimination selection were used to compare the best-fitting models for SSL containing one predictor, two predictors, and so on from some of the variables determined to exhibit a linear relationship with SSL. A final model was selected from these explanatory variables iteratively using a combination of model utility tests, partial F-tests, multicollinearity, and outliers. The final model was selected with parsimony in mind. A parsimonious model explains as much variability in the response as possible without

overbearing complexity. In other words, the model accurately predicts values of the response variable, while incorporating as few predictor variables as possible. A similar selection process was implemented to develop an MLR model predicting SSL from road dimensions alone. Additionally, an MLR model was developed from road dimensions to predict peak flow because peak flow was found to explain a large amount of variability in SSL from the road sites. The following section details the development procedure for the MLR model predicting SSL from road dimensions, turbidity, and runoff, the MLR model predicting SSL from road dimensions, simple linear regression (SLR) model predicting SSL from peak flow, and the MLR model predicting peak flow from road dimensions.

Table 5. List of explanatory variables used in the MLR model selection process to predict road suspended sediment load.

Explanatory Variable	Description
Road length	length of the road segment draining to a flume site (m)
Road width	Average width of the road segment draining to a flume site, including road inside ditch width when applicable (m)
Road area	area of road segment draining to a flume site (m^2), width x length
Slope squared times road length	The slope squared times the road contributing length can be a predictor for road sediment contributions (Luce and Black, 1999) ($m\%^2$)
Cutslope height	Average height of the road cutslope draining to the flume site (m)
Cutslope area	area of the road cutslope draining to the flume site (m^2), cutslope height times length
Cutslope cover	percentage of the road cutslope with soil surface cover from vegetation, woody debris, or litter.
Slope	percent slope of the road segment draining to the flume site
Surface type	surface type of the road segment draining to a flume site, either native or rocked; for the purposes of the MLR, native was coded as 0, while rocked was coded 1
Storm peak flow	maximum storm runoff rate measured (m^3/ 3 hr)
Maximum turbidity	maximum storm runoff turbidity measurement (NTU)
Precipitation	Storm total precipitation (mm)

Multiple Linear Regression (MLR) Incorporating Road Dimensions, Turbidity, and Road Runoff

Prior to carrying out MLR selection procedures and further model development, all explanatory variables from Table 5 were visually assessed using scatterplots for a potential linear relationship with road suspended sediment load (SSL) with the exception of storm, used as a categorical predictor. The data visualization revealed that two Box-Cox transformations were needed to linearize the relationship with SSL. Firstly, SSL was transformed using Log base 10 (Log10) to linearize its relationship with storm peak flow (Figure 10). A cube root transformation was applied to maximum turbidity to linearize the relationship with Log10 SSL (Figure 10). Furthermore, some road physical dimension parameters were eliminated from model consideration before employing the selection procedures because of their lack of a

transformable linear relationship with Log10 SSL. This requirement excluded slope, road length, and road width. The elimination of these parameters from model consideration was further substantiated by goodness of fit tests that suggested a more complex model was needed to fit SSL. This was undesirable in the context of developing a parsimonious MLR model for SSL.

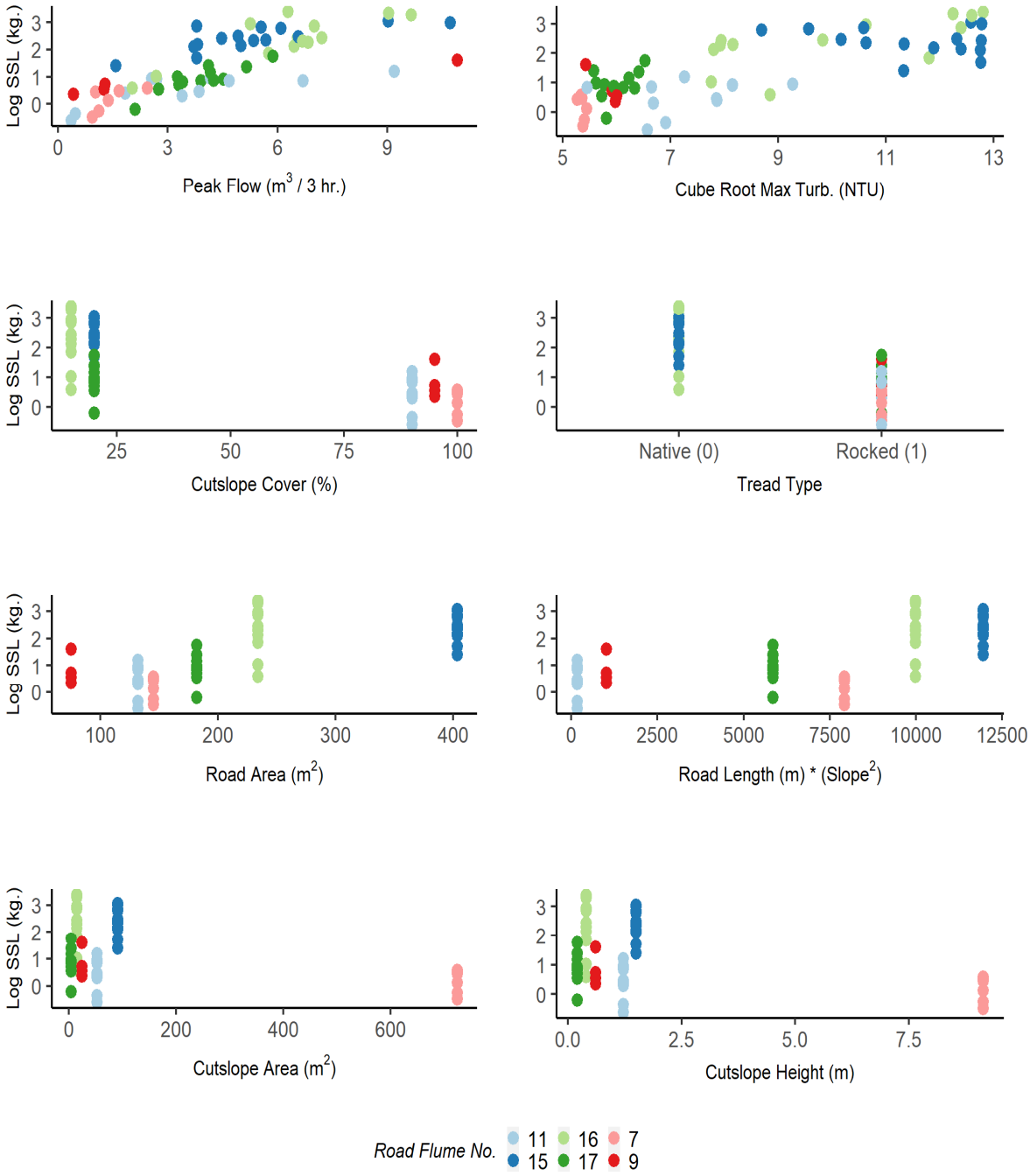

Figure 12. Scatterplots displaying relationship between Log10 road suspended sediment yield (Log SSL) and explanatory variables considered when selecting a model incorporating road dimensions, turbidity, and road runoff.

Multiple Linear Regression (MLR) Incorporating Road Dimensions Only
An identical iterative MLR selection process was used to choose a model fitting Log10 SSL from only road dimension and precipitation variables. In other words without values of turbidity or storm peak flow generated from road runoff measurements. This analysis was to explore what, if any, physical dimensions from the roads provided an indication of suspended sediment production with more readily available information of road dimensions and precipitation. The possible road variables considered for model selection were all those that exhibited a linear relationship with Log10 SSL.

Lastly, an MLR model was fit to storm peak flow from road dimensions and precipitation. The decision to fit this exploratory model was made post hoc to fitting the MLR for Log10 SSL from road dimensions, turbidity, and road runoff. We had an interest in determining if road dimensions predicted the peak flow from road runoff events because the peak flow explained a significant amount of the Log10 SSL variation (see results). Additionally there were considerably more measurements of peak flow than SSL due to the ability to include the crest stage measurements that measured the peak flow from road runoff events but not SSL.

Hydrologic Modelling with the Distributed Hydrology Soil Vegetation Model (DHSVM)

DHSVM Background Information

DHSVM is a physically based, distributed hydrologic model that explicitly solves water and energy balances for each model grid cell (Bowling and Lettenmaier, 2001). DHSVM was originally developed for use in forested, mountainous terrain (Wigmosta et al., 1994) and then extended for use in maritime climates (Storck et al., 1995). DHSVM was modified to assess the influence of forest roads on watershed hydrology (Storck et al., 1995; Storck et al., 1998; Wigmosta & Perkins 2001; Dymond et al., 2014). The model and the road interception component of the model are described in detail elsewhere (Wigmosta et al. 1994; Storck et al. 1995, 1998; Wigmosta & Perkins 2001); thus, only a brief description is provided here.

DHSVM calculates the spatial distribution of soil moisture, snow, evapotranspiration, and runoff in hourly or longer time increments for individual grid cells, or pixels, based on the digital elevation model (DEM) of the watershed. Meteorological inputs required for each time increment of the model are precipitation, relative humidity, air temperature, wind speed, shortwave radiation, and longwave radiation. A one-dimensional water balance is calculated for each grid point based on effects from vegetation, climate, soil hydraulic properties, and topography. The model uses a two-layer canopy representation to calculate interception and evapotranspiration of vegetation, a two-layer energy balance model for snow accumulation and snowmelt, a multilayer unsaturated soil model based on Darcy's Law, and a saturated subsurface flow model. Once the water balance calculations are complete, each grid cell exchanges water with adjacent grid cells, which results in a three-dimensional redistribution of surface and subsurface water across the watershed. DHSVM calculates the amount of overland flow from the road

surface based on the precipitation intensity and infiltration rate of the road surface. Overland flow and intercepted water at the cutslope are routed in the road inside ditch to a drainage structure location.

DHSVM Use for Road Runoff

DHSVM has been shown to provide reasonable estimates of the hydrologic effects of forest roads. Wigmosta and Perkins (2001) demonstrated the utility of the road network component of DHSVM to show changes in peak flows and in the routing of water along road networks for Carnation Creek in British Columbia. Bowling and Lettenmaier (2001) evaluated DHSVM for 12 culverts within Hard and Ware Creeks in Washington and concluded the model simulated outlet and culvert peaks well. The DHSVM model was also used at the Coweeta Hydrologic Laboratory in North Carolina to determine how increasing road density affects average streamflow volumes (Dymond et al., 2014).

Road hydrologic modelling by DHSVM was evaluated using an uncertainty assessment of DHSVM simulations, parameter sensitivity, and the influence of parameter interactions in western Oregon (Surfleet et al., 2010). Results indicated that the use of uncertainty assessment provided a more realistic interpretation of model results by providing a range of acceptable model outputs. DHSVM was further used to evaluate road sediment in western Oregon and northwestern California (Surfleet et al., 2011). The use of DHSVM with road runoff/sediment relationships outperformed contemporary road erosion models (i.e., WARSEM, SEDMODL, and WEPP) and provided sediment yield estimates within 20 to 30% of measured values.

Overview of use

DHSVM was calibrated to South Fork Caspar Creek streamflow. The calibration of DHSVM was through Monte Carlo simulations with randomly selected soil parameters. Models that provided a reasonable fit (called behavioral models) to streamflow identified the final parameter ranges to use for simulations. Statistical relationships between stream and road runoff peak flows and suspended sediment load were developed from measured data. DHSVM road and vegetation inputs were adjusted to provide an evaluation of different harvest scenarios. The scenarios used two separate road networks: (1) The 2018 road network, this includes the roads used for the Phase III harvest primarily along ridges and upper slopes of the watershed for cable yarding, as well as a mid-slope road prior to abandonment, or other JDSF or Mendocino County road segments within the South Fork of Caspar Creek watershed. (2) The Pre-1974 road network with streamside and mid-slope roads designed for tractor yarding. The road scenarios for these two networks represented 2018 CFPR road guidelines with hydrologic disconnection, pre-2010 CFPR road guidelines without hydrologic disconnection, and a pre-1973 CFPR road scenario.

DHSVM Inputs

For input, DHSVM requires (1) spatial information about the watershed in the form of binary grids created from ArcInfo coverages of elevation, soil type, soil depth, and vegetation type; and (2) connecting arcs (spatially aligned lines) for the stream network and road network. A 30-m pixel for South Fork Caspar Creek was projected from LiDAR data with a resolution of two

meters, provided by the USFS PSW. A pixel size of 30-m was chosen because it was an efficient scale for model precision for small watersheds and large enough to encompass the width of stream channels and roads found in South Fork Caspar (a constraint of DHSVM).

Vegetation Inputs

A relationship between stand density index (SDI) and leaf area index (LAI) was developed at Jackson Demonstration State Forest (Berril and O'Hara, 2007). Forest inventory data related basal area with SDI (Webb, 2019), allowing LAI to be interpreted for target basal areas in the South Fork timber harvest for the Phase III experiment. We assumed full ground cover (fractional cover =1) by the forest canopy pre-harvest and scaled the post-harvest fractional cover proportional to forest harvest predictions. The overstory LAI was changed to reflect the reduced post-harvest overstory (Table 6).

Table 6. Leaf area index estimates for pre and post 2017 to 2019 harvest used in DHSVM simulations of the Phase III harvest of the South Fork of Caspar Creek. Information adapted from Jackson Demonstration State Forest (Webb, 2019).

Subwatershed	Pre-Harvest LAI	Pre-Harvest Fractional Cover	Post-Harvest LAI	Post-Harvest Fractional Cover
Ogilvie	7	1	4	0.6
Porter	7.2	1	5.5	0.7
Treat	8.1	1	5.4	0.6
Uqlidisi	6.7	1	3.2	0.5
Ziemer	8.1	1	2.1	0.25
Sequoyah	7.9	1	3.0	0.35
Matrix around subwatersheds	7.0	1	3.5	0.5
Richards (no harvest)	7.0	1	7.0	1
Williams (no harvest)	7.0	1	7.0	1
Yocum (no harvest below Ziemer)	7.0	1	7.0	1

Soil Inputs

DHSVM allows partitioning of subsurface media or soil into different layers based on differing physical and hydraulic parameters. A subsurface media depth of 5-m was used across South Fork Caspar based on soil core depths created for subsurface water studies (Keppeler, 2019). In the 5-m subsurface media a soil depth of 1.8 m was used for the first layer based on maximum depth of soil in the watershed (Rittiman and Thorson, 2006). This chosen depth was similar to hydrologic modelling done in the North Fork of Caspar Creek, which used a 1.5 m soil depth (Carr et al., 2014). The 1.8 – 5.0 m depth was the second layer and considered weathered bedrock, and below 5-m was assumed to be unweathered bedrock. The a priori soil parameters for use in DHSVM were derived from soil hydraulic properties measured in the North Fork of Caspar Creek (Carr et al., 2014), and subsequent modelling using DHSVM and the semi-Lagrangian water temperature model, RBM (Yearsley, 2009, 2012) for South Fork Caspar Creek (Ridgeway, 2019).

Stream Network

The South Fork Caspar stream network for use in DHSVM was generated by the "createstreamnetwork" Python script (Duan, 2017) using a 10,000 m^2 contributing area for runoff generation. This script assigns stream dimensions based on user inputs, and establishes the spatial proximity and routing order of surface water for DHSVM calculations. A variety of contributing areas were evaluated to develop the stream network for DHSVM. The 10,000 m^2 contributing area provided the best simulation of stream segments compared to mapped watercourses used by Jackson Demonstration State Forest staff.

Meteorological Inputs

DHSVM requires meteorological inputs at three hour time steps for air temperature (°C), wind speed (m/s), relative humidity (%), incoming short and longwave radiation (W/m^2), and precipitation (m). The meteorological inputs for DHSVM were developed primarily from one climate station and two precipitation gauges. The meteorological station MET1 (39°21'00" N, -123°44'20" W; on Road 640) and two precipitation stations SFC620 (39°20'29", -123°45' 13") and SFC640 (39°21'05", -123°43'41") are located in the experimental watershed (Figures 2 and 8). The locations of the two precipitation stations were used as meteorological stations in DHSVM to accurately represent the spatial variation of rainfall throughout the watershed.

Most of the meteorological variables needed to run the model (air temperature, wind speed, and relative humidity) were collected in 15-minute intervals. These data were converted to three hour readings by taking the average of the 15-minute readings every three hours. Although PAR (photosynthetically available radiation) data are collected at the meteorological station, actual incoming shortwave radiation measured by the California Irrigation Management Information System (CIMIS) at Windsor Station #103, approximately 100 miles away from the research site, was used to more accurately estimate the amount of shortwave radiation reaching the site (CDWR, 2019). Incoming long-wave solar radiation was computed from the Stefan-Boltzmann equation. Precipitation was measured at Caspar Creek in either instantaneous tips of 0.01 inch or total depth every 15 minutes. To summarize these data into a three hour format, time stamps were rounded to the closest hour and summed for three hour time steps. The resulting sum was converted to meters, as required by DHSVM.

DHSVM Calibration and Parameter Uncertainty Assessment

Streamflow Calibration and Uncertainty

The initial step in the calibration of DHSVM was to conduct a Monte Carlo simulation with randomly selected parameter values sampled over a uniform or previously known distribution. UNIX scripts and DHSVM code efficiencies were created to perform random parameter selection within the Monte Carlo simulations in a parallel computing environment (Adriance, 2018). The randomly selected variables were four soil parameters: (1) lateral hydraulic conductivity, (2) exponent of decay of the decrease in hydraulic conductivity by depth (an exponent of the natural logarithm describing the decrease in hydraulic conductivity by depth of soil), (3) porosity of the soil matrix, and (4) vertical hydraulic conductivity of the surface soil medium (1.8 m in depth). The soil parameters for the >1.8 m depth were based on the fit of previous modelling work at Caspar Creek (Ridgeway, 2019; Carr et al., 2014). The range of soil

parameter values used during the Monte Carlo simulation were based on preliminary model trials that demonstrated competence at achieving model fit to observed data at Caspar Creek and elsewhere (Ridgeway, 2019; Carr et al., 2014; Surfleet et al., 2010; 2011).

In preliminary model runs it was noticed that modification of the precipitation inputs improved model performance. This is likely due to the uncertainty in precipitation measurements, interception and evapotranspiration calculations, and uncertainty in deep groundwater storage and timing not accounted for in DHSVM. We could not apply the precipitation multiplier randomly, so precipitation inputs were varied by a multiplier in increments of 70%, 80%, 100%, 110% of three hour precipitation. Monte Carlo simulations were completed with 2500 model runs for each precipitation modification increment with randomly selected values from the a priori range of the four soil parameters. Ultimately, 10,000 model simulations were used in the Monte Carlo simulations to predict a posterior parameter distribution of our five parameters.

Determination of the posterior parameter ranges was determined by two likelihood functions (goodness of fit statistics): the Nash Sutcliffe Efficiency (NSE) (Equation 1), and the Relative Efficiency (EREL) (Equation 2). The NSE is a common measure of goodness-of-fit for hydrologic models that uses squared residual values making them sensitive to high streamflow events. The EREL value modifies the NSE as relative deviations, adjusting model fit based on size of event, thus better reflecting fit of the entire series and reducing the influence of the absolute differences during high flows (Surfleet and Tullos, 2012). As a result, EREL values are more sensitive to systematic over- or under-prediction, in particular during low flow conditions (Krause et al., 2005). In both functions, higher values within the range of 0 and 1 indicate better fit of the simulation to the measured streamflow.

$$\text{NSE} = 1 - \frac{\sum_{t=1}^{n}(Qs-Qo)^2}{\sum_{t=1}^{n}(\overline{Qs}-Qs)^2} \qquad (1)$$

$$\text{EREL} = 1 - \frac{\sum_{t=1}^{n}\left(\frac{Qs-Qo}{Qo}\right)^2}{\sum_{t=1}^{n}\left(\frac{Qs-\overline{Qo}}{\overline{Qo}}\right)^2} \qquad (2)$$

Where:
- *Qs* = simulated streamflow at time step i
- *Qo* = measured streamflow at time step i
- $\overline{Qs}$ = mean simulated streamflow for time series (time steps 1 to n)
- $\overline{Qo}$ = mean measured streamflow for time series (time steps 1 to n)
- t = 3 hour time step

Behavioral models during the Monte Carlo simulations were determined by achieving high values of both EREL (>0.65) and NSE (>0.65) metrics for simulation of the streamflow observed at the South Fork Caspar Creek weir for 2015 to 2018 hydrologic years (HY) (defined as August 1 – July 30 for Caspar Creek). An NSE of 0.65 has been documented to be an effective target

for hydrologic simulations (Ritter and Muñoz-Carpena, 2013). For all behavioral models, the soil parameter NSE and EREL values were collected for each precipitation increment. The range of soil parameters for behavioral models were summarized (Table 7). The range of NSE and EREL values from the behavioral models for each precipitation increment is shown in Table 8.

Table 7. The a priori and posterior parameter distributions for four soil parameters as input to DHSVM.

Soil Depth (m)	***Porosity***	***Vertical Hydraulic Conductivity (m/s)***	***Exponent of Decay***	***Horizontal Hydraulic Conductivity (m/s)***
A priori	0.35-0.55	$9.0x10^{-5}$ – 0.1	3.0-5.0	$2.2x10^{-5}$ - $1.0x10^{-3}$
Posterior	0.40-0.55	0.001- 0.09	3.5 – 4.5	$9.0x10^{-5}$ - $1.0x10^{-4}$

Table 8. The likelihood function range of the Nash-Sutcliffe Efficiency (NSE) and Relative Efficiency (EREL) for DHSVM fit to South Fork of Caspar Creek weir, 2015-2018 HY.

Function	***70% precipitation***	***80% precipitation***	***100% precipitation***
NSE	0.76 – 0.87	0.86 – 0.89	0.65 – 0.80
EREL	0.92 – 0.97	0.89 – 0.94	0.74 – 0.82

The improved likelihood function values indicate an improvement in model performance by reduction of the precipitation inputs. Attempts at increases to precipitation inputs (e.g., 110% precipitation) gave very poor model performance and were not used. We suggest this reduction in precipitation inputs is compensating for inaccuracies and uncertainty in our inputs for vegetation parameters and deep groundwater storage. The vegetation parameters influence the amount of interception (Reid and Lewis, 2009) and evapotranspiration modelled, while water stored in deep soil or rock layers can change the timing in the water balance.

All precipitation increments produced the same posterior distributions of soil parameters. The posterior range of soil parameters from our Monte Carlo simulations was used for the different model scenarios tested in this study. The South Fork Caspar Creek streamflow output from DHSVM using the range of posterior parameters is compared to measured South Fork Caspar Creek streamflow HY2016 for closer viewing (Figure 13) and for the entire calibration period of HY2015-2018 (Figure 14). A comparison of peak flows from storm events for the South Fork between DHSVM simulated and measured streamflow for the entire calibration period HY2015 to 2018 is also shown (Figure 15). The slope of the linear regression model between the measured and simulated South Fork Caspar Creek peak flows was significantly different from zero (P value <0.001). A 1:1 line representing a perfect fit between the modelled and measured peak flows is shown for comparison.

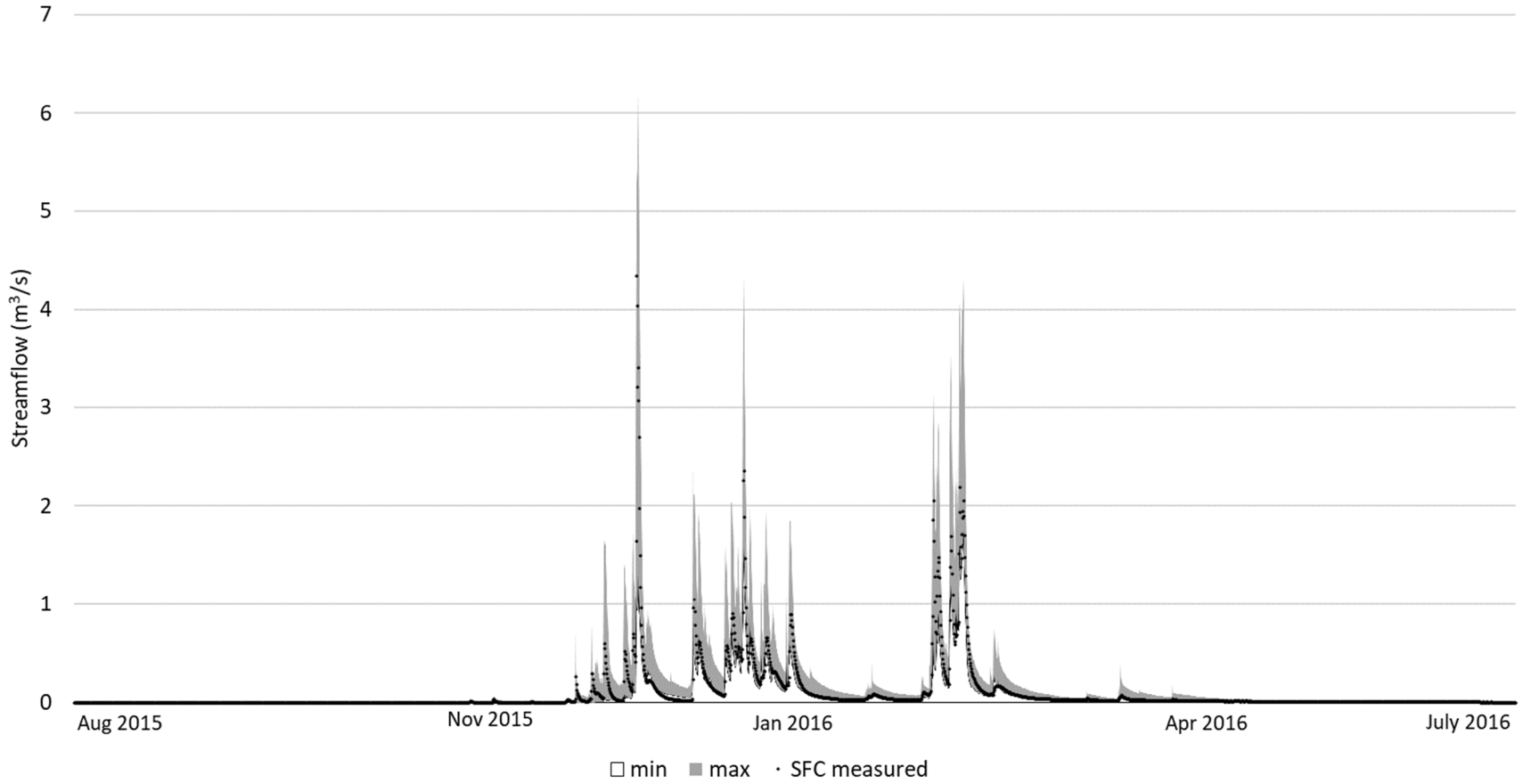

Figure 13. The range of simulated streamflow from DHSVM (greyed area) that provided behavioral models (good fit) to measured streamflow for South Fork Caspar Creek for the 2016 hydrologic year.

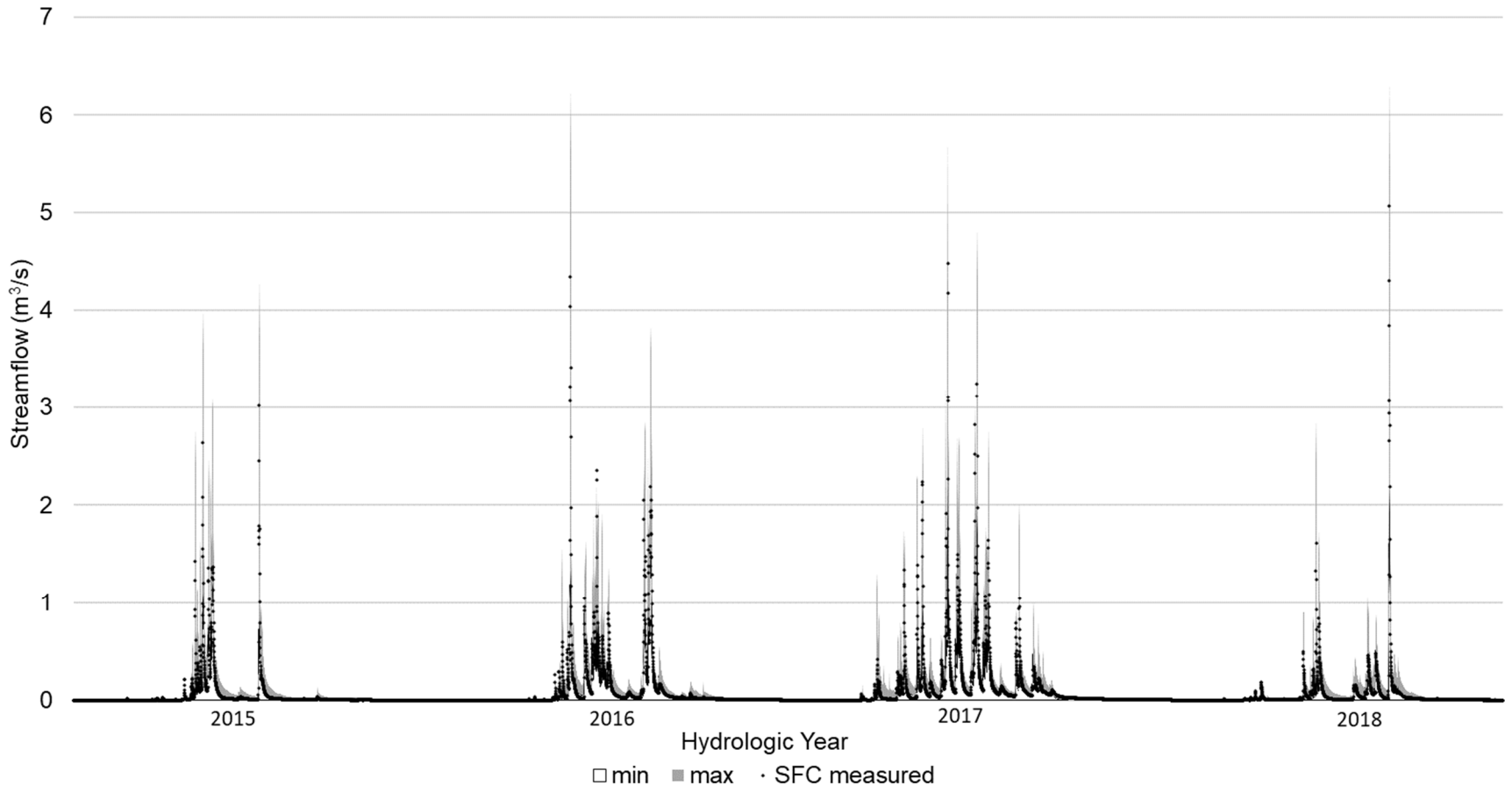

Figure 14. The range of simulated streamflow from DHSVM (greyed area) that provided behavioral models (good fit) to measured streamflow for South Fork Caspar Creek hydrologic years 2015 to 2018.

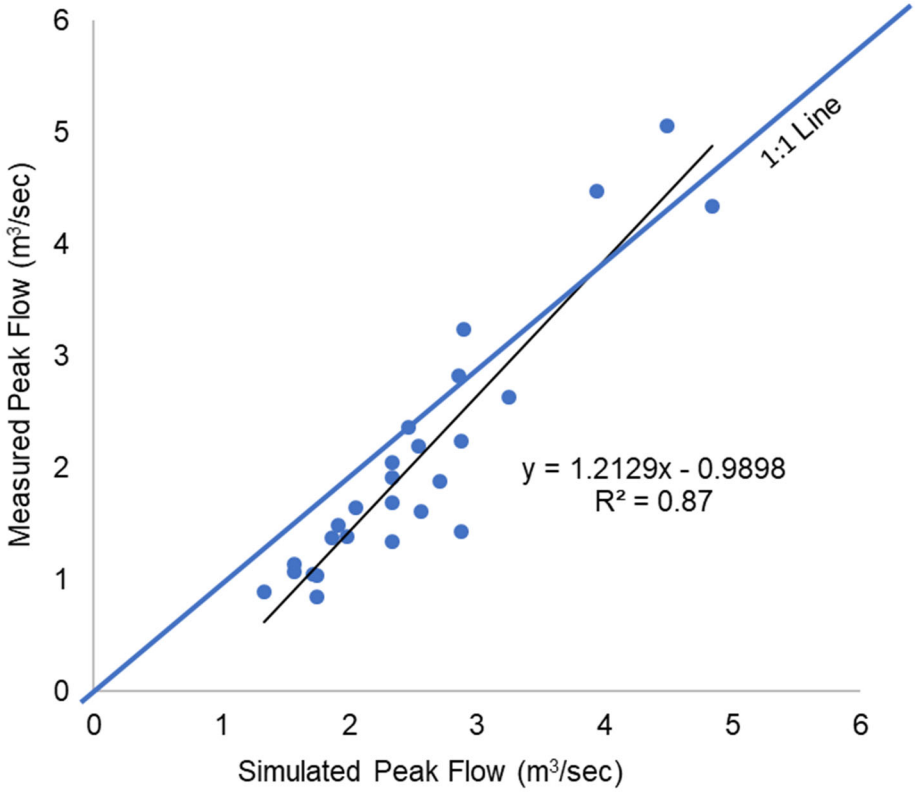

Figure 15. Linear relationship between South Fork Caspar Creek DHSVM simulated peak flow (maximum value of the range of output) and measured peak flow for South Fork Caspar Creek, HY2015 to 2018. The 1:1 line represents a perfect relationship for comparison.

DHSVM Validation for Ziemer Subwatershed

The Monte Carlo simulation produced a range of streamflow outputs that fit South Fork Caspar Creek measured streamflow. The streamflow output from DHSVM for the Ziemer subwatershed (ZIE, Figure 2) using posterior parameters fit to South Fork Caspar Creek is shown for HY2016 (Figure 16) and HY2015-2018 (Figure 17). To validate that fitting parameters for South Fork Caspar Creek works for smaller subwatersheds, the measured streamflow from Ziemer was evaluated for NSE and EREL based on the posterior parameters fit to SFC. The resulting ranges of NSE were 0.22 to 0.50 and EREL 0.68 to 0.88. The NSE shows low to poor fit, while the EREL suggests good fit. This difference suggests the higher magnitude simulated streamflows did not correspond as well to measured streamflow. NSE is biased toward larger events. This was corroborated when looking at the comparison of peak flows from storm events for Ziemer between DHSVM and measured streamflow for the entire calibration period HY2015-2018 (Figure 18).

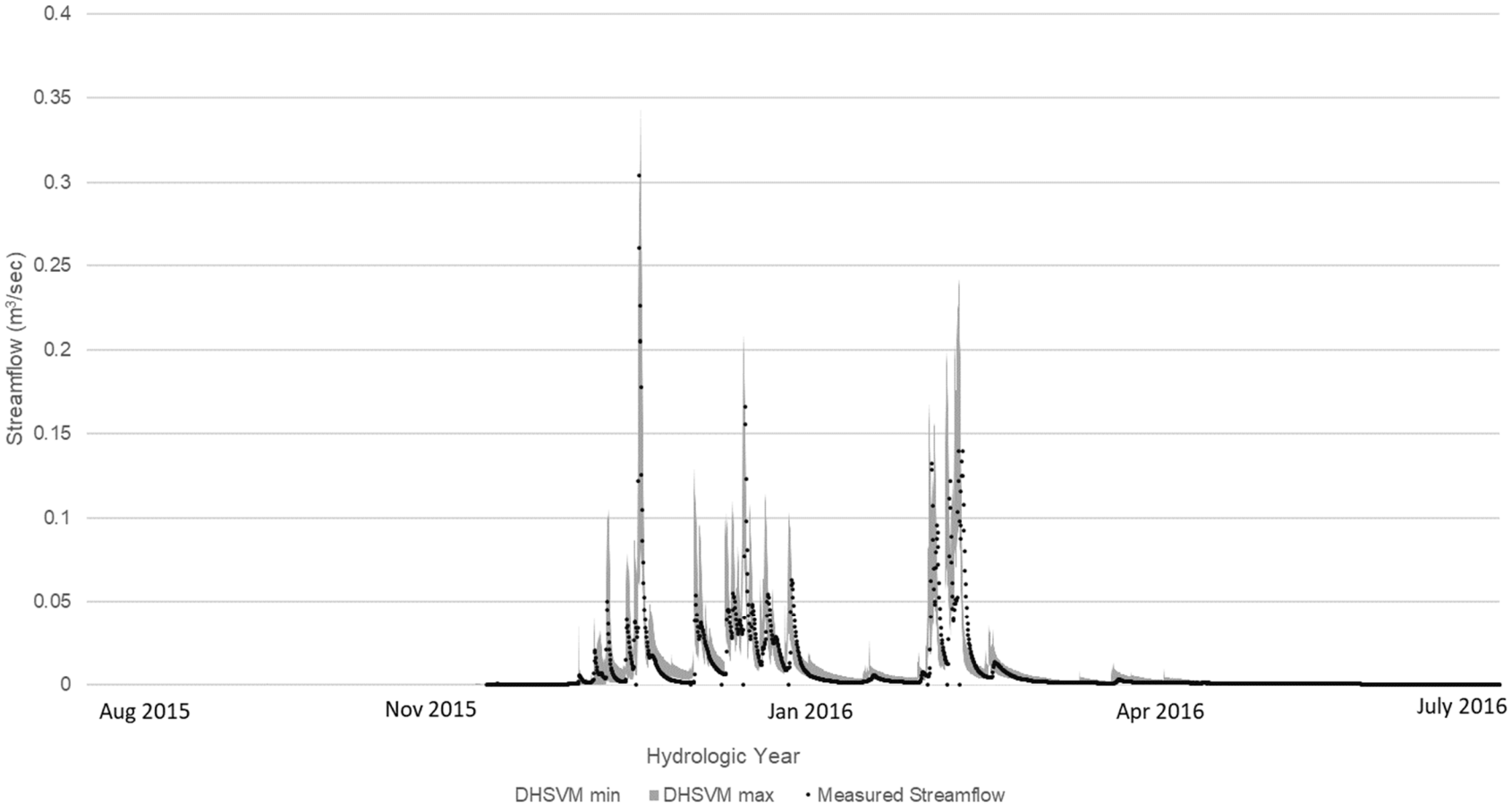

Figure 16. The range of simulated streamflow from DHSVM (greyed area) for the Ziemer subwatershed with parameters providing behavioral models (good fit) to measured streamflow for South Fork Caspar Creek, HY2016.

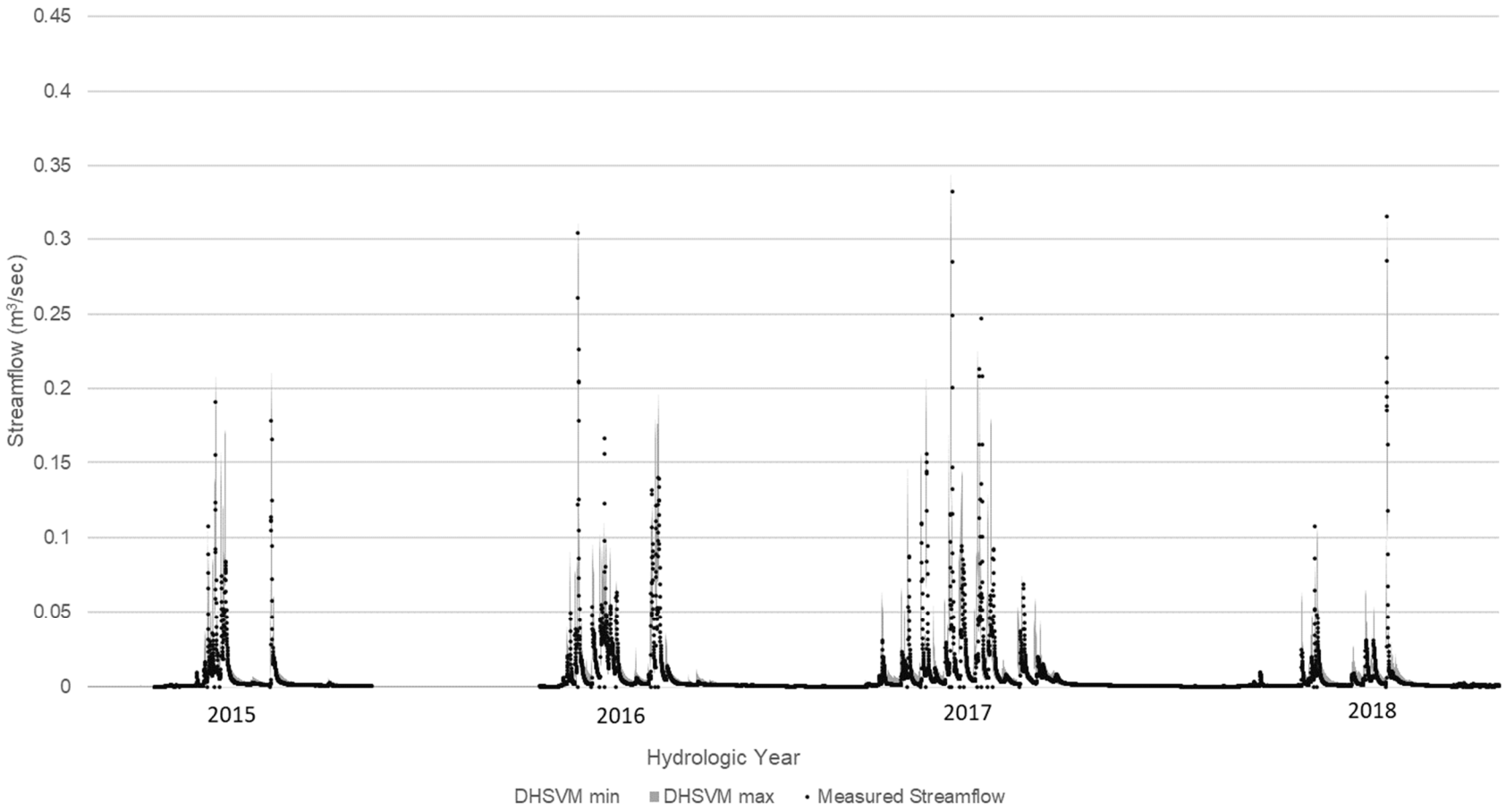

Figure 17. The range of simulated streamflow from DHSVM (greyed area) for the Ziemer subwatershed using parameters that provided behavioral models (good fit) to measured streamflow for South Fork Caspar Creek, HY2015-2018.

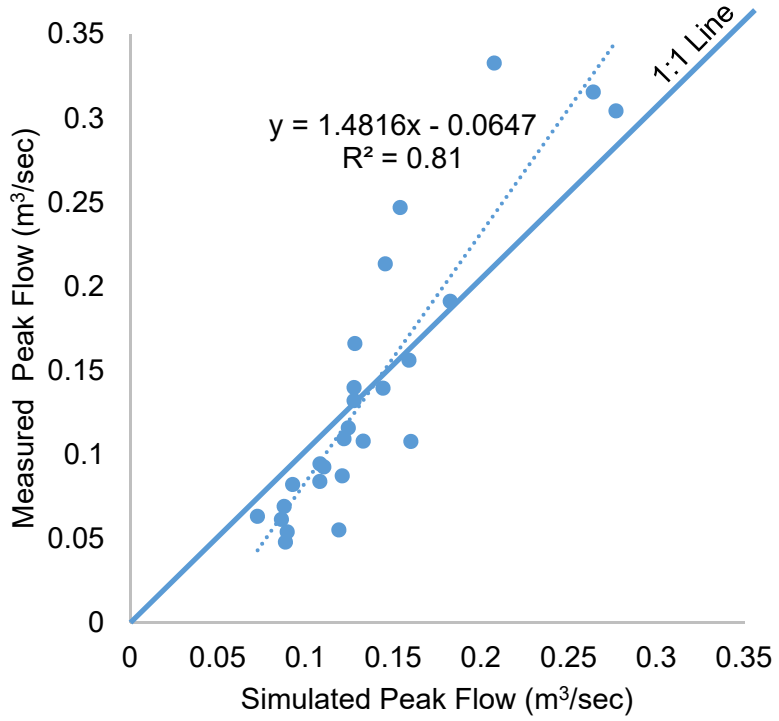

Figure 18. Relationship for DHSVM simulated Ziemer peak flow (maximum value of the range of output) and measured peak flow, HY2015-2018. The 1:1 line represents a perfect relationship for comparison.

Peak Flow to Sediment Load Relationships

An ordinary least squares SLR model was fit between SSL and peak flow for SFC and ZIE using storm and sediment data for hydrologic years 2015 to 2018. There were 27 storms recorded in this timeframe for each basin. To fit the SLR models, sediment load required a Box-Cox transformation to linearize its relationship with storm peak flow. Log base 10 (Log10) was chosen for the transformation. The models were checked for satisfaction of regression assumptions including linearity, error independence, normality, and constant error variance. This SLR process was repeated for the low, median, and high range of peak flows simulated by DHSVM.

DHSVM Road Modelling

The original road network (8.8 km or 5.5 mi) in South Fork Caspar Creek was constructed prior to and during the Phase I harvest, ending in 1973. In 1998, 4.6 km (2.8 mi) of road adjacent to South Fork Caspar Creek watercourses was decommissioned (Keppeler et al. 2007), and in 2011 the mid-slope road segment that traversed the Yocum to Ziemer subwatersheds was similarly decommissioned. The remainder of the mid-slope road traversing the Williams and Uqlidisi subwatersheds was not used in the Phase III harvest and, except for the segment through Williams, was decommissioned as part of the South Fork timber harvesting plan in summer 2019, following this analysis. Several new segments of road were constructed on or near ridge tops to facilitate cable yarding for the South Fork Caspar timber harvesting

conducted from 2017 to 2019. Approximately 4.9 miles of new and 1.9 miles of reconstructed road grade (reconstructing old tractor roads) were built for the Phase III experiment. The 2018 harvest road use occurred during summer and early fall; no winter hauling of logs took place. The roads were winterized following the CFPRs with rolling dips and waterbreaks installed and temporary watercourse crossings removed according to the CFPRs. In some cases, slash was placed on roads adjacent to watercourses for erosion control purposes. Figure 8 shows the road network that existed for the 2017-2019 forest harvesting in South Fork Caspar Creek.

During breaks between storm events in the 2018-2019 winter, the waterbreaks for the existing road network were mapped using a Garmin Montana 600 handheld geographical positioning system (GPS) receiver. The road drainage structure locations defined the road segment lengths that were used as inputs to DHSVM. The calibrated DHSVM model previously used for South Fork Caspar Creek (Ridgeway, 2019) was run with the road network and post-harvest vegetation. The resulting peak flows from DHSVM were compared to the measured road runoff event peak flows. The result showed that DHSVM significantly over predicts peak flows from road runoff, particularly for the largest peak flows (Figure 19). The relationship shows a large amount of deviation from the 1:1 line that demonstrates a perfect relationship between measured and simulated peak flows.

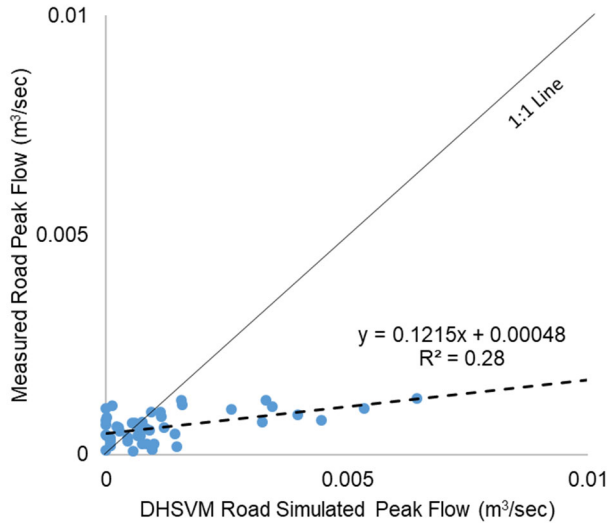

Figure 19. Relationship between measured peak flow from road runoff events from road flumes and simulated peak flows for the same road segments from DHSVM. Road runoff events and road points used were described in Tables 2 and 3. The 1:1 line represents a perfect relationship between the two variables.

The relationship between DHSVM simulated peak flow from road runoff events and measured peak flow is significantly different from zero (p value <0.0001; $R^2 = 0.28$). The equation for the relationship is shown in Figure 19. For evaluation of road runoff, DHSVM generally over predicts the peak runoff. It is speculated that because of the shallow soil depths used in the DHSVM modelling, greater subsurface water is being intercepted by the road cutslope than actually occurs.

DHSVM Modelling Scenarios

DHSVM was run for varying scenarios to evaluate the impact of forest roads and harvest on peak flows and storm sediment loads. The output was evaluated for two watersheds. A small headwater watershed was represented by the Ziemer subwatershed (ZIE), and a larger cumulative impact was evaluated utilizing the entire South Fork Caspar Creek watershed. The range of a priori parameters that produced behavioral model output was randomly selected for 200 model runs per scenario. Each scenario was evaluated for the period August 2014 through April 2019. The Phase III South Fork Caspar Creek forest harvest occurred in the gauged subwatersheds in 2018, however we used the entire time period to evaluate pre-harvest and post-harvest scenarios to provide a greater distribution of storm events. The distribution of output from the 200 model runs for each scenario was isolated into minimum, median, and maximum time series and peak flows for storm events.

In the Phase I harvest of South Fork Caspar (1971 to 1973), a road network designed for tractor logging was developed. This entailed use of streamside and mid-slope roads to facilitate yarding downhill (Figures 20 and 21). This road network had over 400 watercourse crossings and the majority of road segments were adjacent to watercourses. The pre-1974 road network was evaluated with the 2018-post harvest vegetation for comparison to the existing road network. The pre-1974 road network had three scenarios evaluated. The South Fork Caspar road network used in the Phase III harvest had few watercourse crossings or roads adjacent to watercourses. This road network was designed primarily for cable yarding from upper slope spur roads (Figure 21). Using Geographic Information System (GIS) analysis, 21 road segments were identified within 200 feet of classified watercourses. These 21 road segments had waterbreaks installed as per the CFPRs (Table 9). For both road networks different waterbreak spacings were assumed to represent different CFPR requirements.

Figure 20. South Fork Caspar Creek tractor logging—Watershed Sale No. 2—1972 (left); timber stand following Watershed Sale No. 1—1971 (right). CAL FIRE staff photos.

Road modelling scenarios used for each road network (see Table 9; Figure 21):

- 2018 CFPR (with road hydrologic disconnection): road segments with frequent drainage structures or waterbreak spacing for road segments at watercourse crossings (hydrologic disconnection) or within 200 feet of watercourses, as would be required after January 2010, and by the later CFPR road rules package implemented statewide in January 2015.

- Pre-2010 CFPR (without road hydrologic disconnection): road segments reflecting waterbreak spacing as might be found on road networks used prior to the 2009 Anadromous Salmonid Protection (ASP) rule regulations (implemented in January 2010); no hydrologic disconnection requirement. The assumption for this scenario was longer distances between waterbreaks in close proximity to watercourses.

- Pre-1973 CFPR: road segments modelled with few road drainage structures, no winter hauling, little winterization of the roads (John Griffen, JDSF, personal communication, 2020); road practices before the Z'Berg Nejedly Forest Practice Act of 1973 was implemented. All roads had native surfaces. This scenario was only evaluated for the Pre-1974 road network.

- No Roads: the roads were removed from the DHSVM model to allow comparisons between the different road scenarios. It also allowed a comparison between the effect of Phase III forest harvest with and without roads.

Table 9. Road segment lengths and range of lengths at watercourse crossings or within 60 m (200 feet) of a watercourse used in the different scenarios in DHSVM for 2018 and pre-1974 road networks.

Road Network	Road Scenario	Minimum Length m (ft)	Maximum Length m (ft)	Average Length m (ft)	Road Density m/ha (mi/ mi^2)	Percent Road* Length within 60 m of watercourses (200 ft)
2018	2018 CFPR Roads	8 (26)	19 (62)	14 (45)	42.3 (6.8)	13% (3%*)
2018	Pre-2010 Roads**	14 (46)	39 (128)	27 (87)	42.3 (6.8)	13% (3%*)
Pre-1974	2018 CFPR Road Rules	6 (20)	23 (76)	17 (57)	45.7 (7.3)	58%
Pre-1974	Pre-2010 Roads**	14 (46)	35 (115)	24 (92)	45.7 (7.3)	58%
Pre-1974	Pre-1973 CFPRs	186 (610)	317 (1040)	237 (780)	45.7 (7.3)	58%

*- This is the percent of roads used during the harvest operations.
**-These scenarios were based on assumptions of waterbreak spacing required at that time.

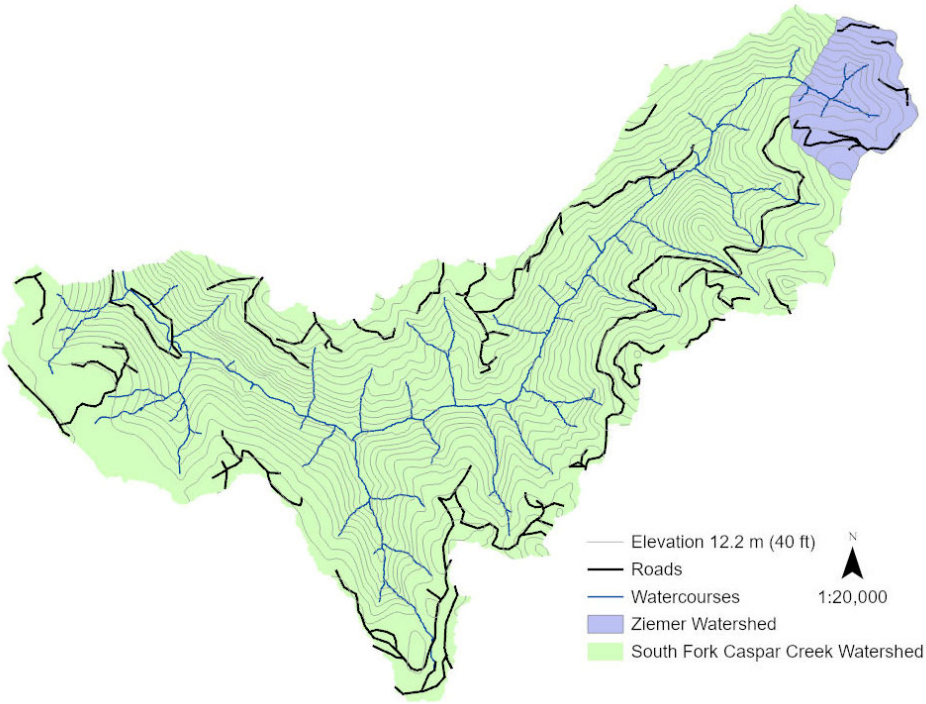

(A)
2018 Road Network

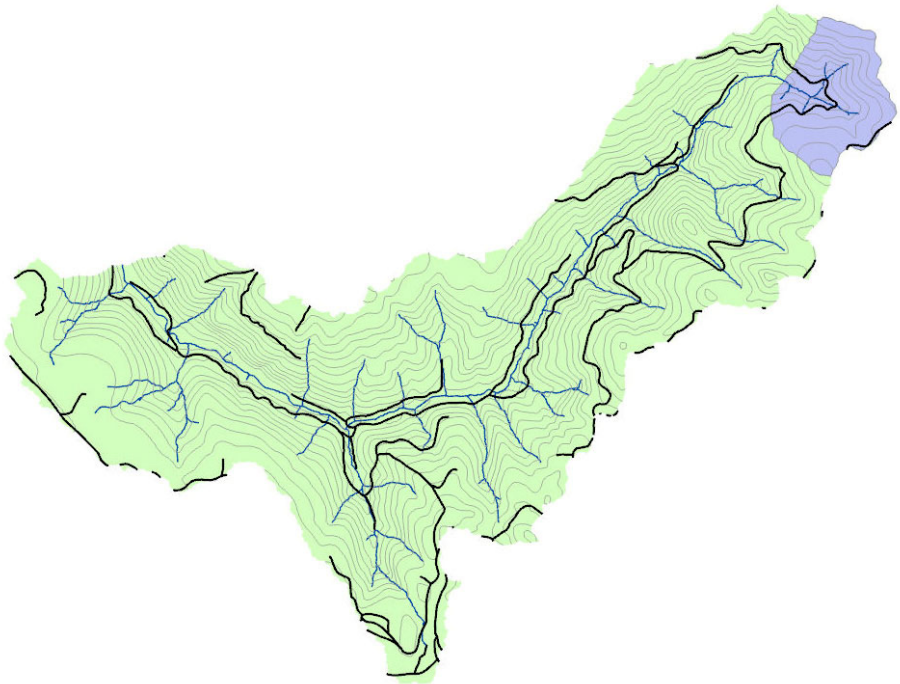

(B)
Pre-1974 Road Network

Figure 21. Road networks evaluated with DHSVM: (A) 2018 and (B) Pre-1974. The 2018 road network was designed for primarily cable logging to upper slope spur roads. The Pre-1974 road network was designed for tractor logging during the pre-modern Forest Practice Rules period with streamside and mid slope roads. A high density of roads in 1970s scenario were directly adjacent to watercourses.

RESULTS

Peak Flow to Suspended Sediment Load Relationships for South Fork Caspar Creek and the Ziemer Subwatershed

Linear Regression of Measured Peak Flow to Suspended Sediment Load (SSL)

A statistically significant relationship was found between South Fork Caspar Creek and Ziemer peak flows and Log10 SSL. The linear regression models for South Fork Caspar Creek and Ziemer are summarized in Table 10. Figure 22 and Figure 23 illustrate the relationship between Log10 SSL and storm peak flow, including the least squares regression line for each watershed.

Table 10. SLR model summaries fitting Log10 sediment load versus peak flow for South Fork Caspar Creek and Ziemer (HY2015-2018), including model regression parameter coefficients, R-squared, adjusted R-squared, sum of squares error (SSE), mean square error (MSE), and number of observations. The parenthesized value under each model parameter coefficient represents the standard error (SE) for the coefficient. ** indicates significance at the 99% level.

	Model	
Parameter	**SFC**	**ZIE**
Constant	3.333** (0.0731)	1.908** (0.102)
Peak flow	0.37** 0.031	5.425** 0.063
R-squared	85.08	74.56
Adjusted R-squared	84.48	73.55
SSE	0.792	1.749
MSE	0.032	0.07
No. observations	27	

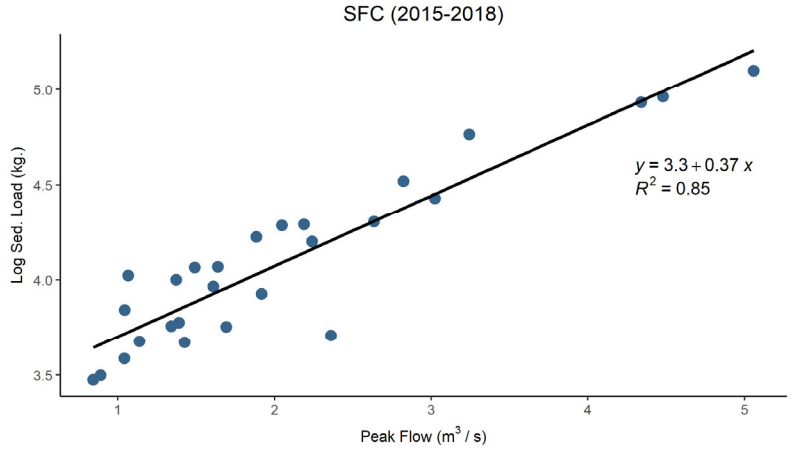

Figure 22. Scatterplot of Log10 sediment load versus peak flow from South Fork Caspar Creek weir (SFC) storm events (HY 2015-2018) including line of best fit, SLR equation, and R-squared.

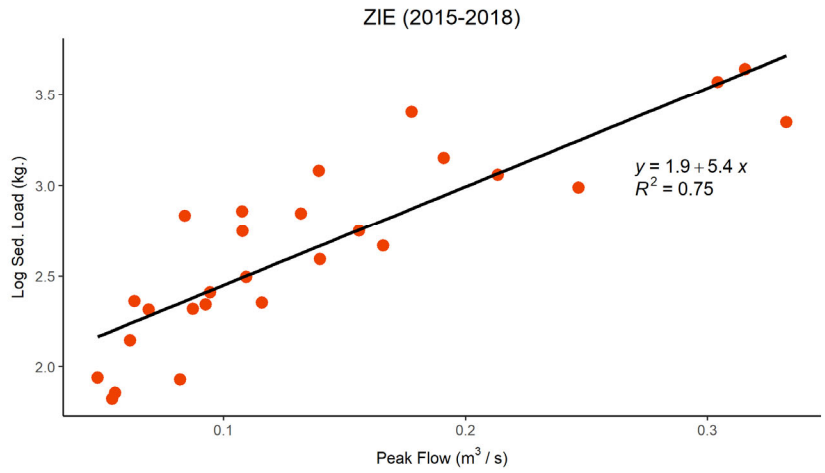

Figure 23. Scatterplot of Log10 sediment load versus peak flow for Ziemer gauge (ZIE) storm events (HY 2015-2018) including line of best fit, SLR equation, and R-squared.

The slopes of the SLR models to predict Log10 SSL from the minimum, median, and maximum DHSVM-modeled peak flows for the South Fork Caspar Creek and Ziemer locations were significantly different than zero (P value < 0.001 in all cases). The SLR equation and R^2 values are shown on the scatter plots for the two watersheds (Figures 24 and 25).

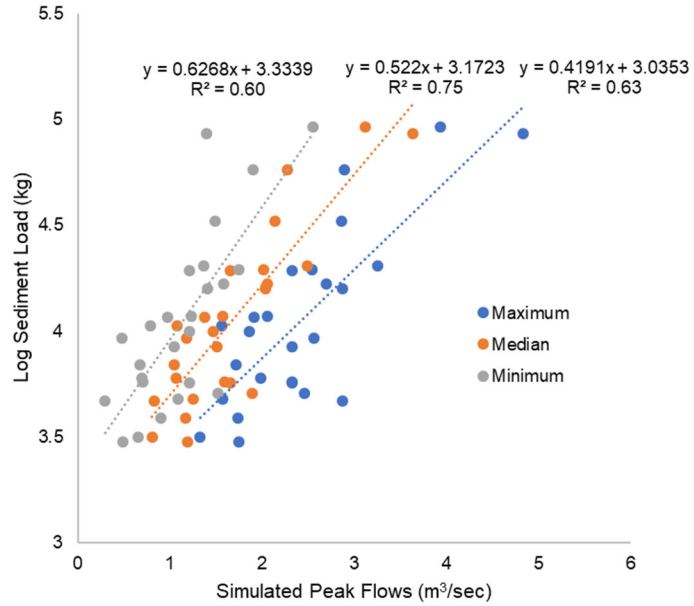

Figure 24. Scatterplot of Log10 sediment load versus the range of peak flows simulated by DHSVM for the South Fork of Caspar Creek storm events (HY2015-2018), including lines of best fit, SLR equations, and R-squared.

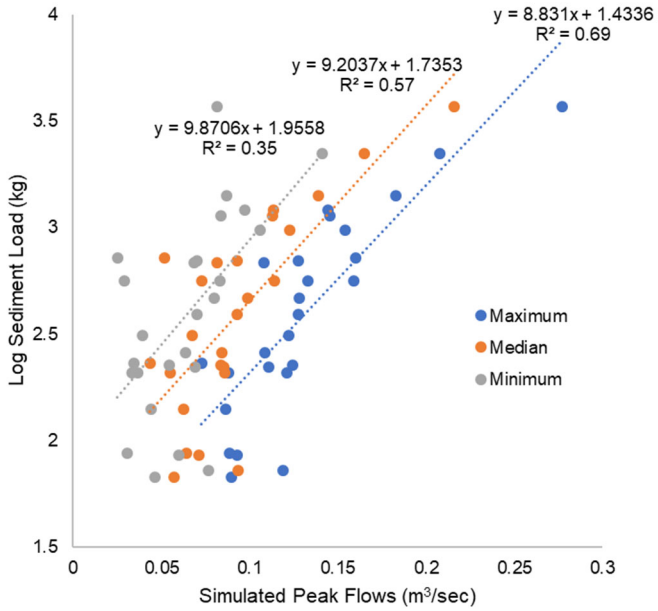

Figure 25. Scatterplot of Log10 sediment load versus the range of peak flows simulated by DHSVM for the Ziemer storm events (HY2015-2018), including lines of best fit, SLR equations, and R-squared.

Multiple Linear Regression (MLR) Incorporating Road Dimensions, Turbidity, and Road Runoff

Best subsets, forward selection, and backward elimination selections for a parsimonious model indicated several candidate models to predict Log10 SSL (Table 11). These models were fit to examine their coefficient of multiple determination (R^2-adj), model utility, and satisfaction of regression assumptions. All candidate models satisfied these assumptions. Partial F-tests were conducted between Model A and both Model B and Model C to determine whether the inclusion of the added variable in each case explained a significant amount of extra variation in SSL. The two partial F-test results are summarized in Table 12.

The results of the partial F-tests show that including cutslope or road surface type in the model explains significantly more variation in Log10 SSL relative to the model including only peak flow and cube root maximum turbidity. Accordingly, the reduced model (Model A) including only peak flow and cube root maximum turbidity was eliminated as a potential best MLR model to predict Log10 SSL. In both Model B and Model C the storm precipitation total was not in the final model selection. Both Model B and Model C were evaluated to detect issues with multicollinearity using scatterplots and variance inflation factor (VIF) values; no model had issue with multicollinearity. Lastly, the two models were evaluated for outliers using studentized deleted residuals and Cook's Distance values. No outliers were discovered to exert leverage on the MLR equation in both models.

Table 11. Candidate model summaries fitting Log10 road suspended sediment load including parameter coefficients with standard error in parenthesis. Coefficients with * and ** indicate significance at the 95% and 99% level, respectively. The adjusted R-squared, sum of squares error (SSE), mean square error (MSE), and the number of observations for each model parameter included.

	Model		
Parameter	A	B	C
Constant	-1.306 (0.202)	-0.538 (0.27)	0.456 (0.413)
Peak flow (m^3/3 hr)	0.2106** (0.027)	0.186** (0.025)	0.192** (0.023)
Cube root max turbidity	0.2159** (0.026)	0.175** (0.025)	0.076* (0.037)
Cutslope cover		-0.007** (0.002)	
Road surface type			-0.935** (0.199)
Adjusted R-squared	80.35	84.14	85.58
SSE	13.06	10.36	9.42
MSE	0.225	0.182	0.165
No. observations	61		

Table 12. Results from partial F-tests including the reduced and full models used in the test, test F-statistic (F*), test F distribution, and test p-value. * indicates a statistically significant partial F-test result at the 95% level in favor of the full model.

Reduced Model	**Full Model**	**F***	**F Distribution**	**p-value**
Model A	Model B	14.88	F (0.95, 1, 56)	<0.0001*
Model A	Model C	22.06	F (0.95, 1, 56)	<0.0001*

Model B and Model C differ statistically in terms of adjusted R-squared values. Neither model departs from MLR assumptions or provides additional prediction power. For these reasons both Model B and Model C are sufficient parsimonious models to predict road suspended sediment yield at the six road flume sites monitored during winter 2018-2019.

In the models that predicted Log10 SSL, road dimensions such as road surface area, cutslope area or height or cover, or road length times slope squared did not improve model prediction power. This was a surprising result and contrary to previous research results (e.g., Luce and Black, 1999; Fu et al., 2010). The question became can the road dimensions produce models that correlated with Log10 SSL or peak flow from road runoff?

Multiple Linear Regression (MLR) Incorporating Road Dimensions with Precipitation

The regression selection procedures using road dimension parameters and precipitation to predict Log10 SSL suggested the best model used length times slope squared, road surface type, cutslope area, and precipitation as explanatory variables (Table 13).

Table 13. Model summary, including parameter coefficients with standard error in parenthesis, fitting Log10 SSL from road dimensions and precipitation. Coefficients with * and ** indicate significance at the 95% and 99% level, respectively. The adjusted R-squared, sum of squares error (SSE), mean square error (MSE), and the number of observations are included.

Parameter	**Best Model**
Constant	1.425** (0.427)
Length times slope squared	6.2e-05** (3.6e-05)
Road surface type	-1.25** (0.274)
Cutslope area	-0.00044** (1.13-04)
Precipitation	0.0076** (0.0013)
Adjusted R-squared	80.7
SSE	12.39
MSE	0.221
No. observations	61

Multiple Linear Regression (MLR) Incorporating Road Dimensions and Storm Fitting Peak Flow

The regression selection procedures using road dimension parameters and precipitation to predict storm peak flow suggested the best model used length times slope squared, cutslope height, and precipitation as explanatory variables.

Table 14. Model summary, including parameter coefficients with standard error in parenthesis, fitting peak flow (m^3/3 hr) by road parameters and precipitation. Coefficients with * and ** indicate significance at the 95% and 99% level, respectively. The adjusted R-squared, sum of squares error (SSE), mean square error (MSE), and the number of observations are included.

Parameter	**Best Model**
Constant	2.274** (0.459)
Length times slope squared	1.89e-04** (5.6e-05)
Cutslope height	-0.1447** (0.0356)
Precipitation	0.0334** (0.0041)
Adjusted R-squared	40.7
SSE	670.72
MSE	5.733
No. observations	125

Road Sediment Predictions from DHSVM Modelled Road Runoff

To predict sediment from roads using DHSVM output we used the guidance provided by the MLR showing a strong relationship between peak flow and road surface type (rocked = 1, native surfaced = 0) to Log10 SSL. We applied this MLR for the range of outputs of road watercourse crossings or road segments within 200 feet of watercourses (n = 21). The relationship between the low, median, and high range of simulated peak flows (m^3/3 hr) and log sediment load for the six road sites with automated sediment measurement were significantly different from zero at 95% confidence (coefficient p values = 0.03 to <0.0001; adj. R^2 = 0.63 to 0.76). The relationships are shown below (Equations 3-5).

Log SSL (kg) = 2.42 + 0.0483 * low peak flows -1.804 * surface type (adj. R^2 = 0.68) (3)
Log SSL (kg) = 2.33 + 0.0342 * median peak flows -1.773 * surface type (adj. R^2 = 0.76) (4)
Log SSL (kg) = 2.25 + 0.0256 * high peak flows -1.724 * surface type (adj. R^2 = 0.63) (5)

The variability of the simulated peak flow to sediment loads coupled with the uncertainty of DHSVM, as represented by the range of streamflow with behavioral models suggest a range of sediment loads should be reported. The relationships for the low, median, and high values of the distribution of peak flows and log sediment load were used to predict total sediment load for the 15 storm events measured from the six road sites (Table 15). The range of total SSL from the DHSVM simulated road peak flows under-predicted the total SSL measured. There were a few very large measured SSL from the native surface roads in this study. The road peak flow to log sediment relationships, although statistically significant for the population of storm events, under predicted these few, very large storm sediment loads. The result was the total measured load was higher than predicted by the DHSVM peak flow to sediment load relationships (Table 15).

Table 15. The total measured load (kg) from six road sites and range of predicted load (kg) by the low-high values of the distribution of DHSVM simulations for the 15 storms in the winter of 2018-2019 with sediment load measured. Note: road measurement sites length varied from 100 to 160 feet (30 to 50 m).

Total Sediment Load Measured (kg)	Range of Total Sediment Load Predicted by DHSVM Peak Flows to Sediment Load (kg)
15,440	10,244 to 12,025

Suspended Sediment Contributions for Different Road Scenarios

The range of average road related and watershed mean annual suspended sediment load (SSL) per hectare of watershed area of South Fork Caspar Creek and Ziemer from DHSVM is shown (Table 16). The estimates use pre- and post-harvest vegetation inputs to DHSVM and the average of HY2015-2019 output (Figures 24-25). The five year simulation period for each scenario provided a varied winter precipitation regime to evaluate the different scenarios.

When simulated with pre-harvest vegetation, the current roads (new road rules) were estimated to deliver a range of 22.8 to 35 kg/ha/yr of suspended sediment for South Fork Caspar Creek (Table 16). The median kg/ha/yr of suspended sediment for the pre-2010 CFPR scenario was estimated to increase by 43.4 kg/ha/yr compared to the 2018 CFPR road scenario. In both

scenarios, 2018 CFPR and pre-2010 CFPR roads, there were slight increases in SSL when simulated with post-harvest vegetation. The comparison of the pre- and post-harvest suspended sediment suggests little change for new roads and a small change for the pre-2010 CFPR road scenarios. This suggests some small increases in runoff with decreased road drainage or waterbreak spacing simulated by the pre-2010 CFPR road scenario.

The pre-1974 road network in South Fork Caspar, built prior to modern CFPRs, had a high density or road length directly adjacent to watercourses. The roads were placed at the bottom of the slope or at mid-slope locations to facilitate tractor yarding, the primary yarding practice of the time in California. The DHSVM simulations for the pre-1973 CFPR road scenarios used post-harvest vegetation from the Phase III harvest as input. The simulations were used to estimate the effect of the pre-1974 road network on suspended sediment if it were to be used today. With the 2018 CFPR road scenario, roads near watercourses must have frequent waterbreaks or other road drainage structures for hydrologic disconnection. Additionally, rocked surfaces would be encouraged on streamside roads to reduce sediment contributions and were included in the analysis. The range of estimated suspended sediment for the new road rules was 346.9 to 469.4 kg/ha/yr (Table 16; Figure 26). The pre-2010 CFPR road scenario simulates less frequent road drainage structures near watercourses than the 2018 CFPR scenario; a rocked surface on the streamside roads was also included in the 2018 and pre-2010 CFPR scenarios. The pre-2010 CFPR road scenario had an estimated suspended sediment delivery range of 409.6 to 594.3 kg/ha/yr contribution. Finally, the estimate using the pre-1974 road network with pre-1973 CFPR scenario, without rocked road surfaces and infrequent road drainage structures, was a range of 954.8 to 2158.2 kg/ha/yr of suspended sediment delivery. In all scenarios the estimated range was wide, demonstrating the uncertainty in our pre-1974 road network simulations. However, it is reasonable to conclude from the pre-1974 road simulations that, even with attempts at hydrologic disconnection of roads and rocked road surfaces, a high density of roads near watercourses produces significant suspended sediment contributions.

The road network used in the Phase III harvest, with 2018 CFPR or pre-2010 CFPR road scenarios and the post-harvest vegetation, shows a slight increase in mean annual sediment load for South Fork Caspar Creek post-harvest (Table 16; Figure 26). The simulation of the South Fork Caspar Creek with the pre-1974 road network using different road scenarios had much larger increases in estimated suspended sediment. As previously mentioned there is greater uncertainty in the simulated output using the pre-1974 road network due to assumptions made about road conditions. There was a general increase in estimated suspended sediment for the pre-1974 road network for the South Fork and Ziemer in all road scenarios (Table 14; Figure 26). Notably the Ziemer subwatershed had a mid-slope road with several watercourse crossings constructed in 1973, later decommissioned in 2011, potentially contributing to the larger increase in SSL in the pre-1974 road network.

Table 16. Suspended sediment contributions for different road scenarios. Values are mean annual suspended sediment load (SSL) per hectare of watershed area estimated from DHSVM simulated peak flow and surface tread type to SSL for roads only, and Mean Annual for South Fork Caspar and Ziemer watersheds (HY2015-2019) using pre- and post-harvest vegetation for different road scenarios.

Forest Vegetation and Road Network	Road Scenario	South Fork Caspar Mean Annual Road Only SSL	South Fork Caspar Mean Annual SSL	Ziemer Mean Annual Road Only SSL	Ziemer Mean Annual SSL
		kg/ha/yr (tons/mi^2/yr)	kg/ha/yr (tons/mi^2/yr)	kg/ha/yr (tons/mi^2/yr)	kg/ha/yr (tons/mi^2/yr)
Pre-harvest Veg.	No Roads	22.8 – 35.0 (6.5 -10.0)	303.7 – 335.5 (86.7 – 96.8)	0	3.7 – 32.2 (1.1 – 9.2)
Post-harvest Veg. 2018 Roads	2018 CFPR	22.9 – 35.1 (6.5 -10.0)	327.7 – 442.8 (93.6 – 126.4)	0	8.1 – 74.9 (2.3 – 21.4)
Post-harvest Veg. 2018 Roads	Pre-2010 CFPR	52.8 – 85.8 (15.1 – 24.5)	396.8 – 583.0 (113.3 – 166.4)	0	10.0 – 98.0 (2.8 – 28.0)
Post-harvest Veg. Pre-1974 Roads	2018 CFPR	346.9 – 469.4 (99 – 134)	650 – 794.0 (185.6 – 226.7)	20.8 – 28.2 (5.9 – 8.1)	38.3 – 297.7 (10.9 – 85.0)
Post-harvest Veg. Pre-1974 Roads	Pre-2010 CFPR	409.6 – 594.3 (116.9 – 169.7)	713.2 – 918.9 (203.6 – 262.3)	24.6 – 35.7 (7.0 – 10.2)	42.8 – 309.8 (12.2 – 88.4)
Post-harvest Veg. Pre-1974 Roads	Pre-1973 CFPR	954.8 – 2158.2 (272.6 – 616.2)	2063.2 – 6282.6 (589.0 – 1793.7)	57.3 – 129.5 (16.4 – 37.0)	123.8 – 377 (35.3 – 107.6)

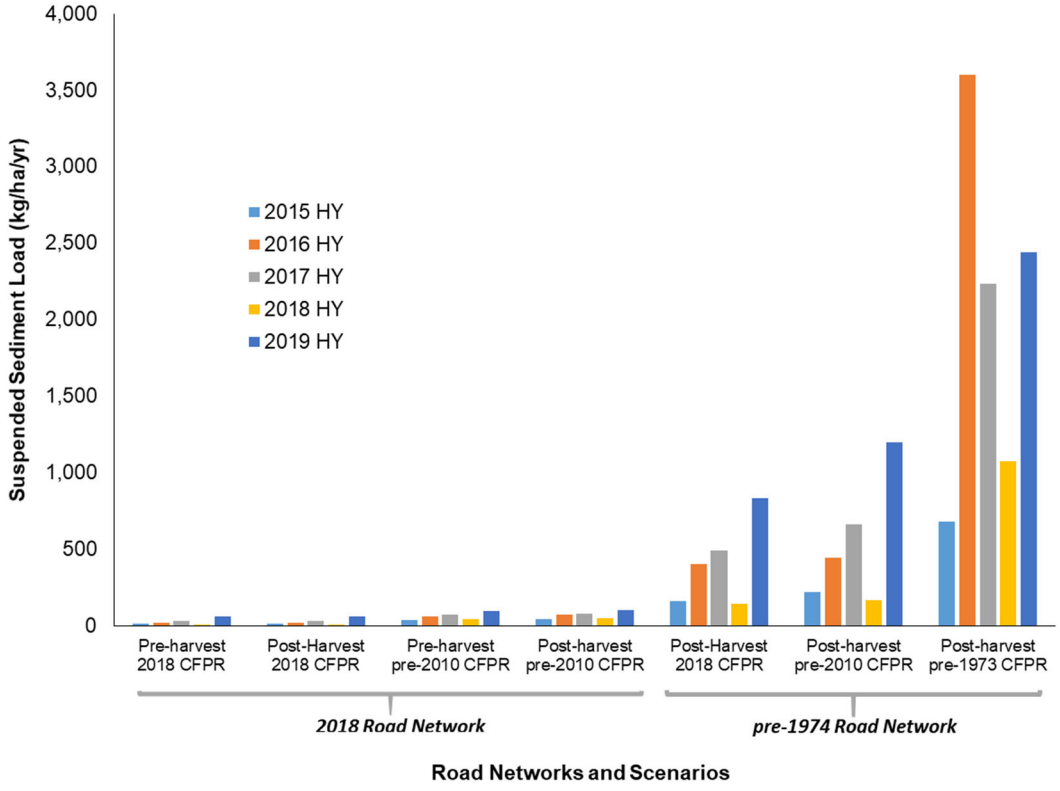

Figure 26. DHSVM-modeled median annual SSL for the South Fork Caspar Creek (HY2015-2019) for different road networks and scenarios.

Forest Harvest and Road Influences on Peak Flows

The relationship between pre- and post-harvest vegetation and different road scenarios was investigated within the range of DHSVM output. The simple linear regression results with the low, median, and high range of DHSVM output from our behavioral models between pre-harvest vegetation and post-harvest vegetation with differing road scenarios were examined for changes in peak flows.

The peak flows of South Fork and Ziemer watersheds increased in response to the Phase III forest harvest compared to pre-harvest vegetation with and without roads as simulated for HY2015-2019 (Table 17; Figure 27). The Phase III forest harvest alone (no roads in the simulation) created a range of peak flow increases from 1.5% – 11% and 2.6% - 17.6% for South Fork and Ziemer, respectively. When the 2018 road network was included in the analysis, South Fork Caspar Creek and Ziemer peak flows were estimated to increase 2.7% to 12.6% and 2.6 to 18%, respectively, using the 2018 CFPR road scenario (Table 17). The forest harvest had the greatest influence on South Fork peak flows. The current road scenario added an additional 1.2% to 1.7% increase in peak flows at the South Fork, while adding a 0.4% increase in the peak flows at Ziemer for the higher range of peak flows predicted. The increase in South Fork and Ziemer peak flows post-harvest were not different using the pre-2010 CFPR road scenario compared to the 2018 CPFR road scenarios.

The South Fork and Ziemer peak flows were estimated to increase 1% to 35% and 5% to 40%, respectively, for the HY2015-2019 with the pre-1974 road network, 2018 CFPR road scenario. The pre-2010 and pre-1973 CFPR scenarios showed even larger ranges of predicted peak flow increases, with the high end of the range of peak flow estimate increasing as much as 46% and 87% for SFC and ZIE, respectively (Table 17).

Table 17. Range of simulated peak flow increases for HY2015-2019 for different road networks and scenarios. Peak flow increases were relative to pre-harvest vegetation, no roads scenario.

Road Network	Scenario	South Fork Caspar Peak Flow Increase	Ziemer Peak Flow Increase
No Roads	No roads	1.5% - 11%	2.6% - 17.6%
2018	2018 CFPR Roads	2.7% - 12.6%	2.6% - 18.0%
2018	Pre-2010 CFPR Roads	2.7% - 12.6%	2.4% - 18.1%
Pre-1974	2018 CFPR Roads	1% - 35%	5% - 40%
Pre-1974	Pre-2010 CFPR Roads	1% - 40%	5% - 53%
Pre-1974	Pre-1973 CFPR Roads	15% - 46%	5% - 87%

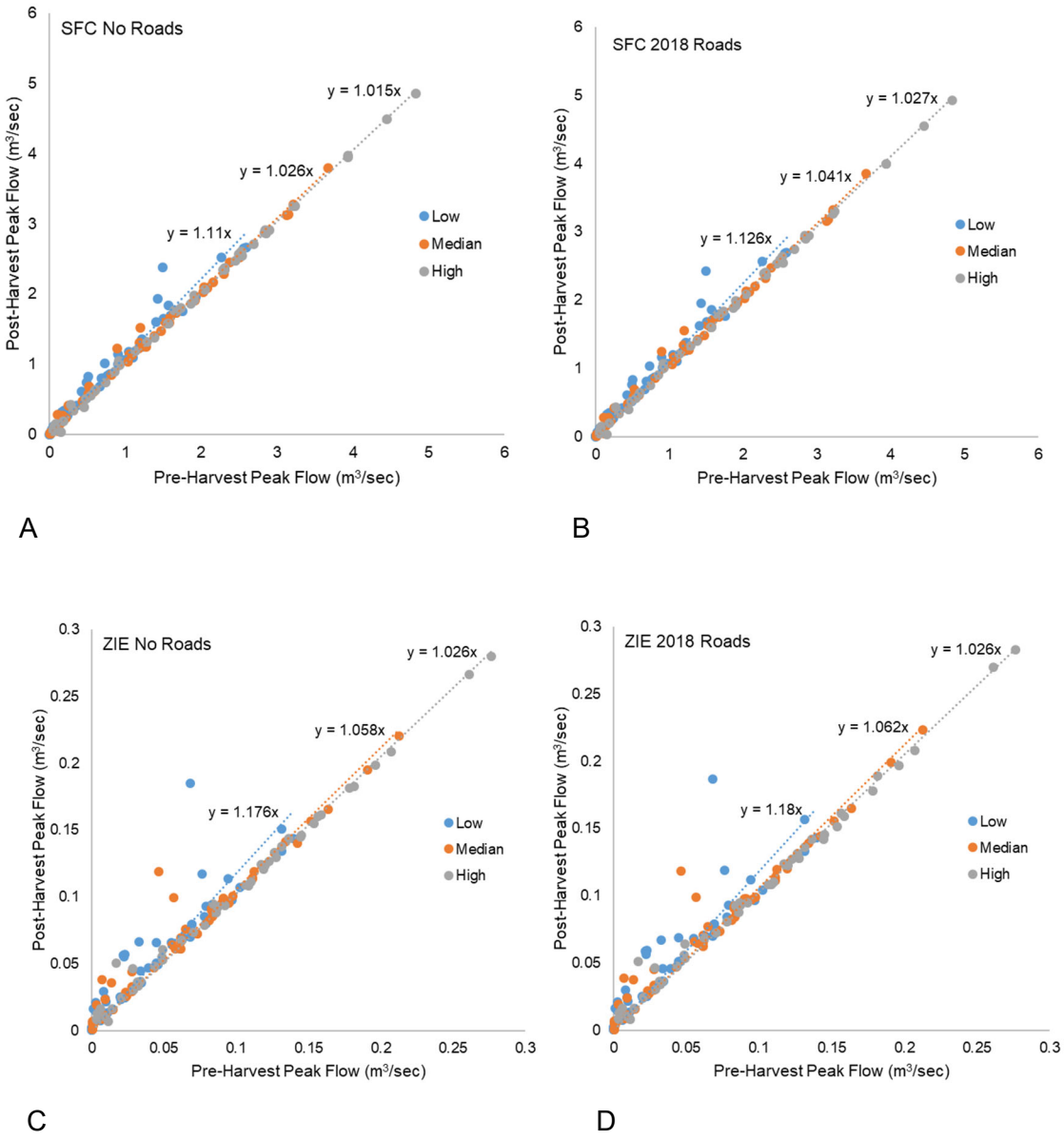

Figure 27. Pre-harvest vs post-harvest peak flows simulated for HY2015-2019 without roads for: A) South Fork of Caspar Creek, C) Ziemer subwatershed. Pre-harvest vs post-harvest peak flows simulated for the HY2015-2019 with the 2018 roads (2018 CFPR Roads) included for: B) South Fork of Caspar Creek, D) Ziemer subwatershed. The trendlines and equations represent the low, median, and high range of DHSVM output. Trendlines had their intercept forced through zero; a slope of 1.0 would indicate no change.

A Log Pearson Type III frequency analysis was created for the South Fork Caspar Creek for annual maximum peak flow from 1967-2019. The return interval and predicted peak flow is shown (Table 18). The highest peak flow during the HY 2015-2019 time period was 5.05 m^3/sec in 2018 HY, an approximate 4-year return interval. The highest peak flow for the South Fork in the 2019 HY, during the field measurement time period, was 4.58 m^3/sec; an approximate 3-year return interval.

Table 18. Log Pearson Type III frequency analysis of the South Fork Caspar Creek annual maximum peak flow for 1967-2019.

Return Interval (yr)	**1.1**	**2**	**5**	**10**	**25**	**50**	**100**
Peak Flow (m^3/sec)	0.66	3.57	5.86	7.43	9.40	10.84	12.26

Case Study - Above and Below Watercourse Crossings

For a case study, a Class I and a Class II watercourse crossing were instrumented for stage at the culvert inlet (Figure 11) and continuous turbidity measurement above and below the crossing. The Class I watercourse crossing (Figure 8; symbol C1) was on Road 600 of Jackson Demonstration State Forest. The other crossing was at a Class II watercourse crossing (C2) on Road 640 (see Table 2 for road dimensions) (Figure 8; symbol C2). Select storm events were monitored from the end of December 2018 to March 5, 2019. The turbidity and stage measurements for the Class I and II watercourses are shown in Figures 28-29.

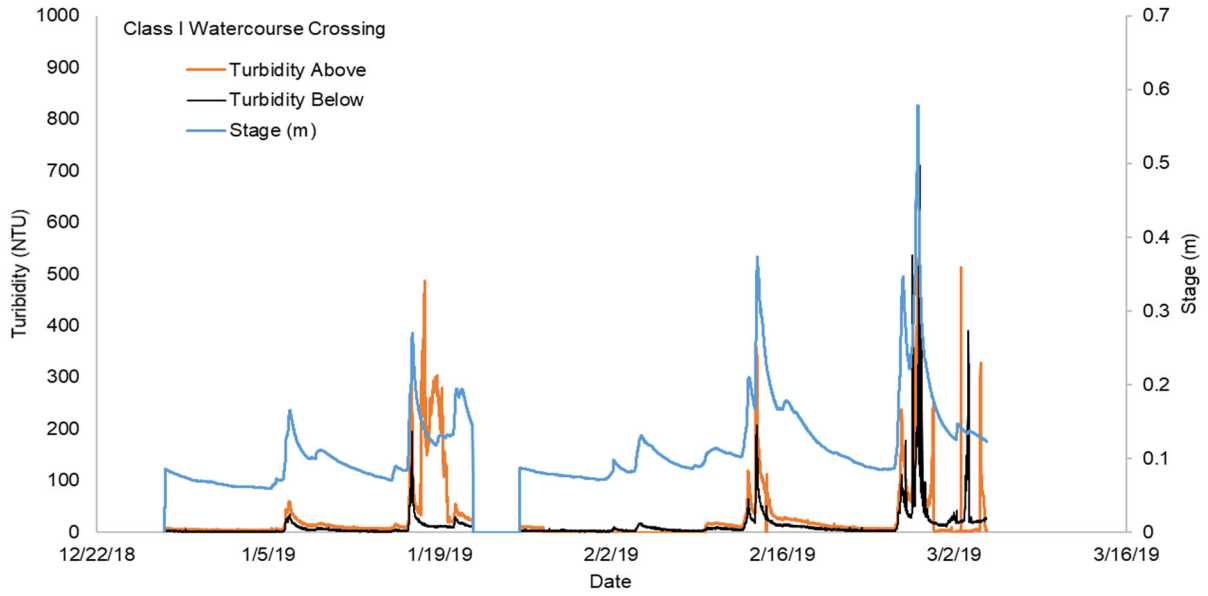

Figure 28. Above and below turbidity measurements and stage at a Class I watercourse crossing on Road 620 of Jackson Demonstration State Forest, December 26, 2018 – March 5, 2019. Break in turbidity and streamflow occurred when upstream turbidity probe placement was changed.

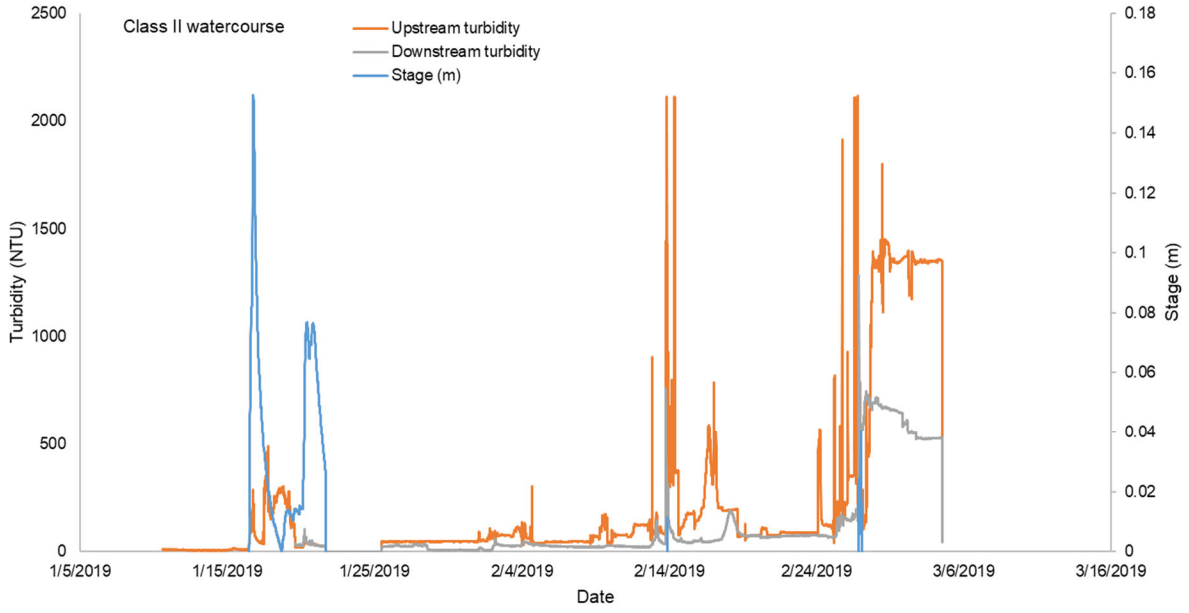

Figure 29. Above and below turbidity measurements and stage at a Class II watercourse crossing on Road 640 of Jackson Demonstration State Forest, January 10, 2019 – March 5, 2019.

The results for both watercourse crossings were inconclusive. Generally, the upstream turbidity was higher than the downstream turbidity for both crossings. The initial installation of the upstream turbidity instrument on the Class I watercourse had problems with sediment deposition due to installation near an eroding streambank. The upstream turbidity meter was moved to a more stable location in late January. The difference in turbidity is noticeable before and after moving the turbidity instrument. In the original configuration the upstream turbidity instrument had substantially higher turbidity compared to the downstream turbidity in the week following the January 16, 2019 peak flow. After moving the upstream turbidity instrument, the upstream and downstream turbidity instrument responded similarly. The upstream turbidity, however, was high throughout February into early March 2019. The exception to this was the peak turbidity in the largest storm event measured on February 27, 2019. In this case the downstream maximum turbidity exceeded the upstream turbidity.

The Class II watercourse proved very difficult to measure (Figures 29-30). The watercourse was steep, >20% in gradient. At the inlet to the culvert the stream grade was lower with rock placed for erosion control. The combination of the rock and gradient change produced a high amount of turbulence in the water column and deposition on the receding stage of streamflow. This was a challenging environment for turbidity and stage measurements. The downstream turbidity probe had similar problems. The steep channel did not have many locations with sufficient water depth for turbidity measurement. The small pool that was chosen had problems

with deposition, burying the turbidity probe. Finally, the above and below crossing sites were not given the top priority for maintenance during storm events.[3]

A B

Figure 30. The inlet and outlet of the Class II watercourse. A) This plate shows the white PVC standpipe at the inlet of the culvert for stage measurement. At the lower left of plate A, in amongst the rock is the turbidity probe. B) This plate shows the outlet of the crossing and demonstrates the steepness of the watercourse. The photographer is standing approximately 20 feet downstream and is 6.1 feet tall and looking up at the outlet.

[3] In a similar above and below watercourse crossing study conducted under road rules in existence in the late 1980s, Cafferata (1989) documented that turbidity increased approximately six times below crossings for five stations located along a poorly surfaced mid-slope road used for winter hauling in the adjacent Hare Creek watershed on JDSF.

Case Study – Side by Side Road Segments with Differing Characteristics

In the statistical analysis of the road sediment load, road surface type (native or rock) was determined to be a predictor variable of road sediment load. Road sites 16 and 17 were selected for measurement in this study because they were side by side with one site having a native surface (Site 16; Figure 31-A) and the other having a rock surface (Site 17; Figure 31-B). Both sites were used for transporting logs from harvest of the ZIE watershed. The contrast between the two sites for the winter of 2018-2019 demonstrates the influence of runoff amount and road surface type on sediment load. The dimensions of the road segments are shown in Table 19.

The average storm runoff was over four times higher for site 16 (native surface) compared to site 17 (rocked), while the total sediment load was over 70 times higher. This difference in sediment yield is indicative of not only the influence of road surface type but preferential flow path contributions to road runoff. The contributing road areas of the two road segments differed by less than 40 m^2 (20 percent) at the measurement point, yet there was considerably more runoff at the native-surfaced site 16. Both sites are within the Ziemer subwatershed adjacent to the Williams watershed divide. A small ephemeral watercourse separates the two sites. Site 16 (native surface), on the north side of the watercourse, is further into the Ziemer subwatershed and influenced by more upslope area for potential subsurface preferential flow contributions. Site 17 (rocked) was directly adjacent to the watershed divide (trees visible in Figure 31 B represent the watershed divide).

Table 19. Road dimensions, average storm runoff, and total sediment load (kg) for road sites 16 and 17; November 2018 - March, 2019.

Dimension	Site 16	Site 17
Length m (ft)	39 (128)	26 (85)
Avg. Width m (ft)	6 (19.7)	7 (23)
Surface area m^2 (ft^2)	234 (2517)	182 (1958)
Cutslope cover (%)	15	20
Slope (%)	16	15
Surface Type	Native	Rock
Average storm runoff m^3 (ft^3)	145.7 (1568)	33 (255)
Total Sediment Load kg (tons)	1410.9 (1.56)	19.6 (0.02)

A

B

Figure 31. Road sites 16 and 17 with road runoff, turbidity, and suspended sediment samples within the Ziemer subwatershed. Both images are looking from near the top of the road segments downhill. The white PVC flumes at the bottom of the segments are the measurement locations for each segment.

A) Road site 16 is a native surface road;

B) Road site 17 is a rocked surface road (see Figure 8 for location of sites within Ziemer subwatershed).

The influence of preferential flow paths in the form of large soil macropores (soil pipes) is well-documented in Caspar Creek watersheds (Ziemer, 1992; Keppeler and Brown, 1998). Numerous soil pipes were observed in the road cuts along the road network above road site 16, suggesting a greater runoff potential for the site following forest harvest. Weathered sandstone parent material was also particularly shallow in this area and was observed in the site 16 road segment. The sandstone in and around SFC weathers to a low-permeability argillic horizon conducive to generation of excess overland flow. The low level of runoff at site 17 compared to site 16 suggests higher permeability, but the road's rocked surface obscured direct observation of the underlying soil.

DISCUSSION

Road Measurements Influencing Suspended Sediment Load (SSL)

The best model to predict Log10 SSL from road runoff events included peak flow, maximum turbidity, and either cutslope cover or road surface type (native or rocked) (Table 11). The additional explanatory variables are both associated with cover of soil on the road surface or cutslope. This suggests efforts to obtain cover on the road surface or road prism during or following use is important to reduce erosion and sediment yield. Road dimensions of area, cutslope height or area, or length times slope squared (Luce and Black, 1998) did not improve model fit to predict Log10 SSL when road runoff variables were included (peak flow, max turbidity).

Road erosion models such as WEPP:Road, Washington Surface Erosion Model, or SEDMODL rely heavily on inputs of precipitation and road dimensions of length, width, slope, and road cover to estimate road sediment production. Additionally, the CFPRs (Technical Rule Addendum No. 5, CAL FIRE, 2020) stress the importance of decreasing road segment length or area to achieve hydrologic disconnection and subsequent reduction of sediment delivery of roads. Because of this road dimensions and precipitation, without runoff variables of peak flow or turbidity, were examined to determine if they might predict Log10 SSL.

The MLR model that best predicted Log10 SSL from road runoff events included event precipitation and road dimensions of road length times slope squared, road surface type, and cutslope area (Table 13). This model explained 80.7% of the variability in Log10 SSL. In comparison the best model with storm peak flow, maximum turbidity, and road cutslope or road surface type explained 85-86% of the variability in Log10 SSL. Luce and Black (1998) demonstrated that road length times slope squared had a theoretical and measured correlation with road sediment contributions. In addition, the model includes the road surface type, an indicator of road surface cover. The road statistical results influencing SSL bear a similarity to a contemporary study (Brown et al., 2013) that investigated the major forest road characteristics that govern rates of sediment delivery in the Virginia Piedmont. Brown et al. (2013) found that road approach length and bare soil percentage were the most important factors controlling measured sediment delivery.

Cutslope area had a negative relationship with Log10 SSL in the MLR using precipitation and road dimensions. In other words a greater cutslope area would reduce SSL. This can be explained by cutslope area being highly influenced by topographic position of the road. Generally roads with the highest cutslope area were: (1) at the top of the slope or ridge, away from watercourses, allowing longer road lengths between road drainage points; or (2) bisecting ridges in the lower portions of the canyon. In both situations this diminished the influence of an upslope contributing area on road runoff, explaining the lower SSL from this study's road measurements. Near the top of the ridge there was little area for subsurface flow paths to accumulate water and be intercepted by the road. Roads that crossed a ridge required a greater cut into the slope to maintain a direct road alignment (Figure 32). This often occurred on roads toward the bottom of the canyon. The road cuts that bisected ridge topography had

little upslope contributing area for subsurface flow accumulation to be intercepted by the road. Rather, subsurface flow paths are directed away from the ridges. Conversely, the roads with the lower cutslope area tended to be the steeper, upper slope roads which had little cover, generally steep slopes, and high energy runoff producing greater SSL.

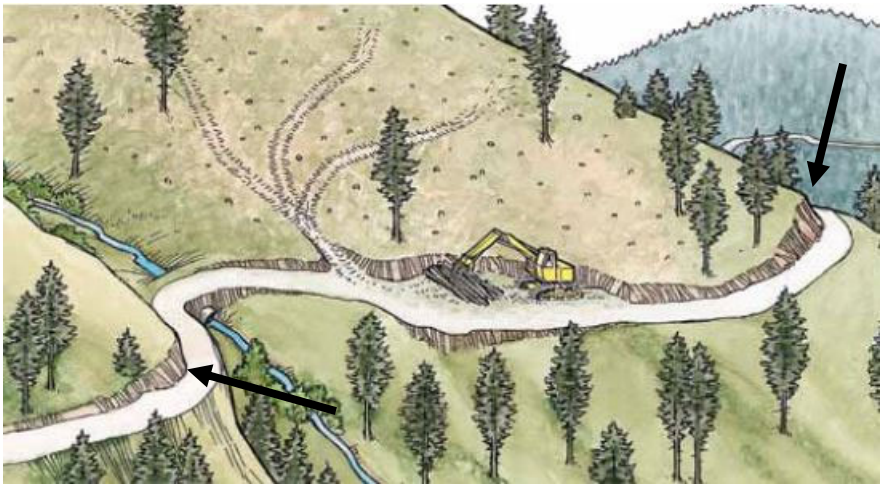

Figure 32. An illustration of larger road cutslope height and area when roads cross ridge topography (indicated by arrows) compared to road cutslopes adjacent to the watercourse (Image from Oregon Forest Resources Institute, 2011).

Lastly, the influence of maximum storm turbidity on Log SSL provides some potential guidance on assessing the water quality impacts from forest roads. Grab samples at the road sites during high intensity precipitation or close to the storm peak flow could potentially indicate the magnitude of road suspended sediment load. In a study on road suspended sediment yield (Surfleet et al., 2011), prediction of the SSL for the largest storm of a winter was correlated with the total annual SSL. If grab samples are taken across road points, indications of the major suspended sediment sources could be identified for potential treatment. However, for this to be successful, considerable planning would be needed in addition to forecasts of large storm events. Ideally it would be useful if a low-cost technique could be developed that would allow quantification of the peak turbidity level, much as is done with crest-stage gauges for identification of the maximum storm peak flow.

Road Dimensions Affecting Peak Flows

The road dimensions combined with precipitation that provided the best MLR to predict road runoff peak flows were road length times slope squared and cutslope height (Table 14). In contrast to the MLR using road dimensions to predict Log10 SSL, road cutslope height slightly improved the model over road cutslope area, a predictor of SSL. However both have the same negative correction with peak flow, in other words as cutslope height increases the peak flow response decreases. Like cutslope area the predictor cutslope height was highly influenced by topographic position of the road. Roads with steeper slopes, as indicated by the length times slope squared term in the model, had smaller cutslopes in our sample of roads in South Fork Caspar Creek. Road cutslope cover was not a predictor in the best model to predict road runoff peak flow. The amount of bare soil on a cutslope was important for predicting SSL, however it

did not affect the peak flow from the road runoff. In the MLR model predicting peak flow from road dimensions and precipitation there were far more roads measured, providing a greater sample of road response. The subtle differences in road dimensions predicting either peak flows or SSL could be a function of the different sample sizes.

Watershed Effects of Roads on Suspended Sediment

South Fork Caspar Creek roads constructed for the Phase III experiment timber sale should be considered a best case scenario for a coastal California forest land base. Only ridgetop or upper-slope spur roads were used for the yarding and forest harvest. Much of the pre-1974 road network in the watershed has been decommissioned or was not used. The Phase III experiment 2018 road network resulted in low estimated levels of suspended sediment delivered to watercourses (22.8 to 73.5 kg/ha/yr), based on the range from the two road scenarios evaluated. Only 20 road segments in the 2018 road network, 3% of the 2018 road network length, were within 60 m (200 feet) of watercourses; 10 of the 20 road segments crossed watercourses. In contrast the pre-1974 road network had 58% of the road segments within 60 m (200 ft) based on the stream network created for DHSVM input. Rice et al. (1979) stated approximately 75% of the pre-1974 road network in South Fork Caspar occupied areas within 60 m (200 ft) of watercourses.

Frequent waterbreaks to promote hydrologic disconnection of the roads, required in the 2018 CFPRs for hydrologic disconnection, were installed prior to winter thus reducing suspended sediment contributions. Additionally, only pre-existing, all-season roads were used during the winter season when the majority of precipitation occurs. The frequent waterbreak spacing created by hydrologic disconnection, as simulated for the 2018 CFPR road scenario, produced less suspended sediment than the pre-2010 road scenario where hydrologic disconnection was not required (and assumed not implemented). The median difference was approximately 30 kg/ha/yr.

The pre-1974 road network scenarios for South Fork Caspar represent a likely scenario for coastal California. Legacy road networks throughout coastal California were created to facilitate historic logging practices. Although not the case at Caspar Creek, many coastal watersheds had historic railroad logging that required low grades, keeping railways low on the slope, often within stream channels. As railroad transport of logs was replaced by truck transport, existing railroad grades were often converted to truck roads, keeping the transportation network close to the bottom of canyons and near watercourses. Much of the second growth forest in coastal California was harvested in the post-WWII housing boom for the United States using ground based tractor logging. This type of yarding was most efficient with a high density road network on mid-slopes and canyon bottoms, as found in the pre-1974 road network of South Fork Caspar Creek. It was more cost effective to yard logs downhill, often along ephemeral or intermittent watercourses, to reduce fuel costs and increase production. Many of the watersheds in coastal California still have elements of these legacy road networks. South Fork Caspar Creek had a particularly high density of streamside roads in the pre-1974 road network, in some cases running up both sides of the mainstem creek (Figures 33 and 34csurflee).

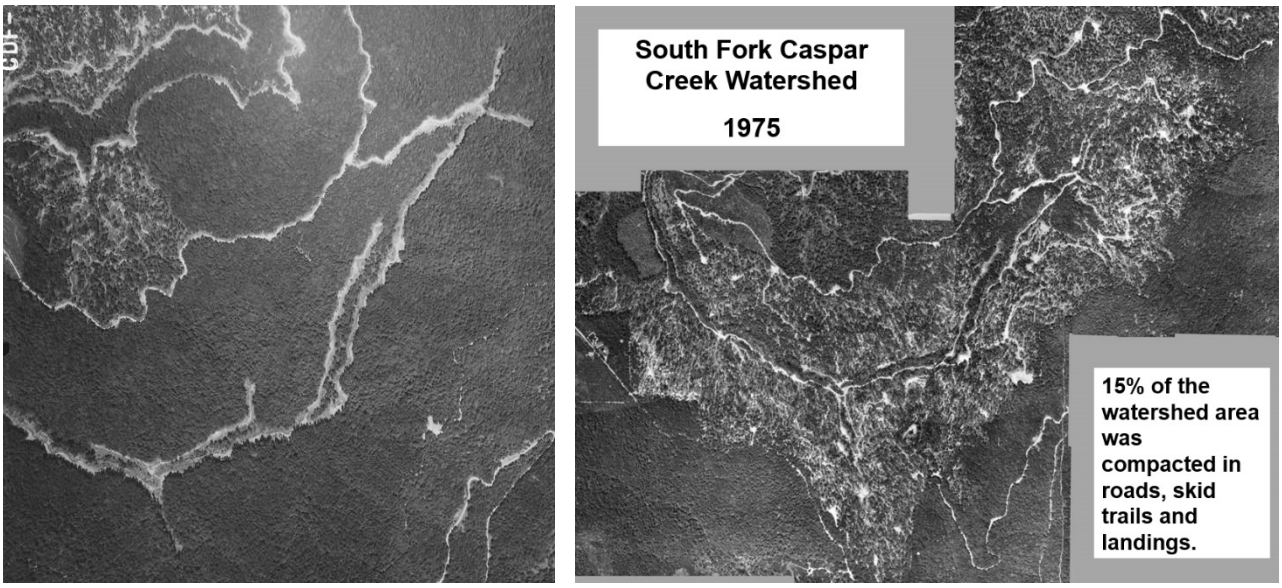

Figure 33. South Fork of Caspar Creek in 1968 after initial road construction (left), and the South Fork in 1975, after tractor logging and final road construction (source: USFS PSW).

Figure 34. South Fork Caspar Creek roads used in timber harvesting completed from 1971 to 1973. Note native surface roads on both sides of the South Fork watercourse (photo taken in the early 1970s by James Burns, DFG; a similar photo is included in Burns, 1972).

Our attempt to simulate the Phase I road network in the watershed used a pre-CFPR road scenario. All road surfaces were assumed to be native surface roads with infrequent road drainage structures or waterbreaks. The range of road SSL delivered to watercourses was

estimated to be 954.8 to 2158.2 kg/ha/yr. In contrast, other studies estimated 1403 kg/ha/yr (Rice et al., 1979) and 1475 kg/ha/yr (Lewis, 1998) for the first year after road construction. The DHSVM generated estimate envelopes these totals, however with much greater uncertainty.

The pre-1974 road network was simulated using a modified road drainage structure spacing as mandated under the 2018 CFPRs (hydrologic disconnection) and pre-2010 scenarios (no hydrologic disconnection). Additionally, these scenarios assumed rocked road surfaces for the segments adjacent to the mainstem creek. Using a 2018 CFPR scenario, the range of road sediment delivered to watercourses was estimated to be 346.9 to 469.4 kg/ha/yr. This scenario reduced sediment delivery from the pre-1974 road network by approximately 65 to 79%, based on the range of estimates. Using a simulated pre-2010 road scenario, with rocked road surfaces adjacent to the mainstem, the range of road sediment delivered to watercourses was estimated to be 409.6 to 594.3 kg/ha/yr. In both 2018 CFPR and pre-2010 CFPR scenarios for the pre-1974 road network, sediment delivery was reduced from the pre-1973 CFPR scenario estimates, however there was still considerable road sediment delivery. This suggests that even with current CFPR road practices, road networks with a high density of roads adjacent to watercourses will continue to produce significant sediment delivery. In this study we estimated almost 10 times more sediment delivery from the pre-1974 road network compared to the 2018 road network using 2018 CFPR requirements.

Comparison to a Previous Road Study at Jackson Demonstration State Forest

A road surface erosion study was conducted on Jackson Demonstration State Forest (Barrett et al. 2012) evaluating 10 road segments with varying characteristics. All four of the rocked road segments were located in the Caspar Creek watershed (Roads 600, 620, and 640). The mean annual SSL was normalized by road area; the native surface roads contributed 0.1 to 4.5 $kg/m^2/yr$, while rock surface roads produced 0.02 to 0.8 $kg/m^2/yr$. In the current study, using the six roads that had suspended sediment measured, we determined that native surface roads contributed 17.8 to 41.0 $kg/m^2/yr$, while rock surface roads produced 0.01 – 0.85 $kg/m^2/yr$. The rock surface road SSL determined for this study and Barrett et al. (2012) SSL were similar. The rocked surface roads in this study did not have high levels of road traffic or any harvest traffic during the wet season. The estimate of SSL from the native surface roads in this study was considerably higher than that reported in the Barrett et al. (2012) study. One explanation is that recently constructed roads or roads used for recent harvesting have greater erosion rates due to the recent soil disturbance (e.g. Reid and Dunne, 1984; Megahan and Kidd, 1972; Coe, 2006). All of the native surface roads in the Barrett et al. (2012) study were older, well established roads with very limited or no recent logging disturbance (JDSF Roads 90, 210, 240, 1000). Reid and Dunne (1984) reported 130 times greater sediment from heavily used roads while Megahan and Kidd (1972) found a 750 fold increase in sediment production from roads following construction. In a study of forest roads in the central Sierra Nevada, Coe (2006) showed recently graded roads had 3 to 4 times higher sediment production when compared to ungraded roads, and that there was a 16-fold difference in median sediment production rates between rocked and native surfaced road segments.

Peak Flow Changes due to Forest Harvest and Roads

The 2017 to 2019 forest harvest, excluding roads, was predicted to increase peak flows by a range of 1.5% to 11% for South Fork Caspar Creek compared to no roads and pre-harvest vegetation for the 2015 to 2019 precipitation regime. The forest harvest in the smaller Ziemer subwatershed was predicted to increase peak flows by a range of 2.6% to 17.6% (Table 17). The 2017 to 2019 forest harvest removed an approximate 42% of the basal area in South Fork Caspar, while basal area removal in Ziemer was 71%. The greater proportion of forest harvested explains the greater increases in the estimated peak flows at the Ziemer subwatershed. In their analysis of the North Fork of Caspar Creek peak flows (Caspar Creek Phase II), Lewis et al. (2001) found similar results, where the proportion of the watershed harvested influenced the magnitude of peak flow increase. Their study could not relate watershed size to a change in peak flow.

The 2018 road network with the 2018 CFPR and pre-2010 CFPR scenarios increased peak flows less than 2% for South Fork Caspar Creek and less than 1% for the Ziemer subwatershed. Both scenarios had few watercourse crossings and a low proportion of roads close (<60 m; 200 ft) to watercourses (3% within 60 m). Forest roads alter watershed hydrology from creation of infiltration excess overland flow from compacted road surfaces and interception of subsurface flow paths at road cuts (e.g., Reid and Dunne, 1984; Luce, 2002; Wemple and Grant, 1996). This influence was captured in our road runoff measurements; however, the general hydrologic disconnection of the 2018 road network produced only a small change to the South Fork and Ziemer peak flows.

The pre-1974 road network was simulated by DHSVM to have a very wide range of peak flow change. South Fork Caspar Creek peak flows were estimated to increase by 1 to 35%, 1 to 40%, or 15 to 46%, depending on 2018 CFPR road, pre-2010 road, or pre-1973 CFPR road scenarios, respectively (Table 17). The pre-1974 road network runoff was modelled with the 2018 post-harvest vegetation; some of the predicted increase could be from the reduction in vegetation from forest harvest. The high amount of streamside roads or roads in close proximity to watercourses would suggest an acceleration of runoff to watercourses, which elevated the downstream peak flow.

The estimated increase in peak flow for the Ziemer subwatershed was greater than for South Fork Caspar Creek. In the pre-1974 road network, a mid-slope road traversed the Ziemer subwatershed over relatively steep terrain (Figures 21B). The estimated range of peak flow increase for the Ziemer subwatershed was 5 to 40%, 5 to 53%, or 5 to 87%, depending on 2018 CFPR, pre-2010 CFPR, or pre-1973 CFPR road scenarios, respectively. The range of peak flow increases progressively increased with decreases in waterbreak spacing and road drainage structures, as shown by the different road scenarios. For the pre-1973 CFPR scenario, peak flows were predicted to increase by as much as 87%. Although a very large change, this scenario is simulating road contributing lengths with direct drainage to the watercourse in several locations with road lengths over 200 to 300 m (650 to 1000 ft) in length. The watershed is small (25 ha or 62 ac) creating a scenario where accelerated water inputs from long road approaches would produce larger peak flows.

Road Hydrologic Disconnection and Cumulative Watershed Effects

The Phase I and II experiments of the Caspar Creek watershed study demonstrated changes in peak flows and suspended sediment following forest harvest (e.g., Rice et al., 1979; Lewis et al., 2001; Ziemer, 1998b; Reid, 2012). This study of the Phase III 2017 to 2019 forest harvest of South Fork Caspar Creek has modeled changes in peak flows from the forest harvest (Figure 27; Table 17). The technique used to estimate suspended sediment for the SFC and ZIE monitoring stations was the relationship between storm peak flow and suspended sediment load. In this approach, a shift in peak flow will lead to a predicted increase in the estimated suspended sediment load (Table 16, Figure 26). The impacts of peak flow increases do have a direct influence on increased suspended sediment through accelerated channel erosion, as observed in the Phase II study in the North Fork of Caspar Creek (Reid et al., 2010; Lewis et al., 2001). Increased peak flows from forest roads have been documented to accelerate erosion in other studies (e.g., Surfleet et al., 2011). In this 2017 to 2019 forest harvest, the combination of increased peak flows and forest road influences was estimated to have increased the suspended sediment output for South Fork Caspar Creek by 24 to 107.3 kg/ha/yr (Table 16) for the 2018 CFPR scenario. For the same 2017 to 2019 post-harvest current road scenario, the smaller Ziemer subwatershed was estimated to have an increase in suspended sediment ranging from 4.4 to 42.7 kg/ha/yr. For both the South Fork Caspar and Ziemer watersheds, the increase in peak flow predicted the increase in SSL, a finding consistent with Lewis et. al (2001). Comparatively, using annual sediment loads and the South Fork as the control, the North Fork Caspar Creek harvest from 1989 to 1992 increased SSL for the six years post-harvest by 118 kg/ha/yr, a 28% increase over pre-harvest load (Lewis, 1998). This comparison must be qualified by the fact that the estimates were created by two different methods (modeling and direct measurement) and time periods. However, the high range of SSL increase estimated for the recent South Fork harvest (107.3 kg/ha/yr) approaches this North Fork value. The range of estimated increase in the South Fork Caspar Creek post-harvest SSL with the new road rule scenario was 8% to 32%. The North Fork Caspar Creek, using unlogged North Fork subwatersheds as controls (a more sensitive analysis), experienced a larger SSL increase of 89% compared to pre-harvest (Lewis, 1998; Lewis et al., 2001). However, the tributaries of the North Fork Caspar Creek experienced an even larger SSL increase of 123 - 269% compared to pre-harvest (Lewis et al, 2001). The Ziemer subwatershed, tributary to SFC, had a 43% to 212% modeled increase in the estimated range of SSL post-harvest.

When the pre-1974 road network is paired with pre-1973 CFPR road scenario, SSL for South Fork Caspar Creek was estimated to range from 2063 – 6283 kg/ha/yr. This represents a 1759 – 5947 kg/ha/yr increase from a pre-harvest no road estimate. In contrast, the 1971 to 1973 forest harvest was predicted to have an increase in SSL of 3245 kg/ha, as reported by Rice et al. (1979) or 2877 kg/ha/yr reported by Lewis (1998). The range of SSL increase from this study bracketed these estimates. However, there was considerable uncertainty in the pre-1974 road network, since the time period and subsequent climate inputs were different and the 2018 post-harvest vegetation was used in the DHSVM simulations. Lewis (1998) and Lewis et. al (2001) estimated a 1475 kg/ha/yr increase in SSL due to road construction, 51% of the SSL. This study estimated an increase of the post-harvest SSL for the pre-1973 CFPR road scenario

to be 34% to 46%. The high end of the range in SSL predicted here is higher than that presented in Lewis (1998) but the proportion of the total increase is slightly lower.

The SSL load increases in South Fork Caspar Creek and Ziemer following the Phase III harvest, as estimated in this study, were primarily due to the change in peak flow increasing SSL. The 2018 road network with current CFPR road rules and road placement away from watercourses contributed less than 20% of the predicted SSL increases in the South Fork. In the Ziemer subwatershed, road contributions provided no SSL increases for the 2018 harvest for both 2018 CFPR and pre-2010 CFPR road scenarios. For the pre-1974 road network and pre-1973 CFPR scenario, roads contributed a high proportion of the total SSL in the Ziemer subwatershed.

The different road scenarios modelled were influential to cumulative watershed effects. The 2018 CFPR road scenario predicted lower sediment than the pre-2010 road rule scenario for both the 2018 and the pre-1974 road networks. The 2018 road rule scenario further decreased SSL compared in the pre-1974 road network to 22% - 36% of the pre-1974 road scenario. However, even with this reduction in SSL, contributions for the 2018 CFPR rule scenario on the pre-1974 road network were approximately 10 times larger than the same scenario on the 2018 road network with upper-slope locations away from watercourses.

The SSL and peak flow changes estimated for South Fork Caspar Creek used a range of road standards from the 2018 road network to the pre-1974 near-stream, inadequately drained, road network. It is likely that these road network configurations demonstrate the end points of the spectrum of road configurations found on private forestland in coastal California. The 2018 road network represents the state-of-the art in road design using current regulatory standards. While some private forestlands in California still have many mid-sloped and streamside roads, this study shows an improvement in suspended sediment contributions may be achieved using the CFPR road rules requiring hydrologic disconnection (e.g. 2018 CFPRs).

Uncertainty in DHSVM at Caspar Creek

Hydrologic modelling is a useful tool for assessing impacts from land management or climate disturbances. Inherent in model structures are assumptions of the processes that simulate a water balance. Additionally, the parameters and forcing data for models come with further assumptions and errors. Other applications of DHSVM have shown uncertainty in model output (e.g., Surfleet et al., 2010) that must be understood to provide reasonable interpretations of model output.

DHSVM solves water balances at small scales typical of digital elevation models distributed across a watershed for short time durations. In this way it can be a powerful tool for simulating time series hydrologic data. The routing of subsurface water assumes a decreasing hydraulic conductivity with depth through a soil matrix. Caspar Creek does have downslope matrix subsurface flow; however, many of the hillslopes also have significant preferential flow paths from soil piping. The influence of preferential flow paths is to accelerate subsurface water routing when soil surrounding soil pipes becomes saturated. This threshold behavior can alter peak flow timing, magnitude, and hydrograph recession for select storm events. The model

structure of DHSVM does not simulate this process. The calibration of DHSVM provided good fit to the South Fork Caspar Creek time series, however individual storm hydrographs or smaller subwatershed responses were not as accurate.

Model uncertainty was estimated by varying influential soil hydraulic parameters in DHSVM. The range of soil parameters that were shown to provide behavioral models had random selections for the different simulations provided. Small differences in model output did result due to this randomization; however, the output was within the limits of our chosen likelihood functions of NSE and EREL values greater than 0.65, where 1.0 indicates perfect fit. Due to efficiency problems with a high computational demand model like DHSVM, other parameters influencing evapotranspiration and vegetation characteristics were not adjusted. Additionally, long term storage of water in deeper soil or rock layers were not represented. To compensate for this the precipitation input to DHSVM was varied from 70% to 100% of measured values. This range was selected by trial and error, with adjustments to precipitation not improving model fit outside this range. The 70% and 80% precipitation inputs produced the best fitting models to South Fork Caspar Creek streamflow, with NSE and EREL values ranging from 0.76 – 0.89 and 0.89 – 0.97, respectively. Measured precipitation, 100% precipitation input, had NSE and EREL ranges of 0.65 – 0.80 and 0.75 – 0.82, respectively. We assume this difference is due to deeper groundwater storage or evaporation underestimated by DHSVM.

The road model within DHSVM assumes road cuts intercept hillslope water when the saturated depth reaches the base of the road cutslope. DHSVM's road model also includes calculation of overland flow based on precipitation intensity and user specified road infiltration rates. This road simulation did not accurately predict the measured road runoff in South Fork Caspar Creek. DHSVM tended to under-predict runoff from small precipitation events and over-predict higher precipitation events. However, there was a statistically significant linear regression relationship with DHSVM road simulated peak flows and SSL. We assume this compensates for the road model bias from DHSVM. In larger storm events the modelled road influence on watershed peak flows could be greater than what actually occurs. This could influence our estimates of peak flows, particularly for the pre-1974 road network, where roads had a large influence on accelerated SSL and peak flows. With the 2018 road network, roads had little influence on watershed peak flows. This suggests that the road influence on peak flows from the 2018 road network could be over-estimated, implying our results represent a conservation estimate of impact.

Simulated results for all of the scenarios for the pre-1974 road network had much greater uncertainty associated with them because of insufficient data on road drainage. DHSVM simulates road interactions with watershed hydrology in a similar manner as the stream network. This created instability in the modelling of the streamside roads for the pre-1974 road network in South Fork Caspar Creek. For example, drainage spacing often intersected stream crossings before the prescribed spacing was achieved. The result was a much greater range of output for the pre-1974 road network simulations. However, the range of output for the pre-1974 road network simulations bracketed the estimates of SSL determined with the actual Phase I harvest and road construction in South Fork Caspar Creek. The climate inputs and

post-harvest vegetation were not the same, but it does suggest that the magnitude of the differences in the road scenarios for the legacy road network were reasonable.

CONCLUSIONS

Statistical analysis of measured road segments indicated the most efficient model to predict suspended sediment load was the maximum turbidity and peak flow of storm events. The model was improved by including measures of soil exposure, road surface type (rocked or native surfaced) or cutslope cover percentage. The results indicate that road network monitoring that captures peak flow events would give reasonable estimates of the magnitude of road suspended sediment contribution. It further illustrates the need to cover exposed soils on roads for reduced surface erosion and suspended sediment. Using only precipitation and road dimensions, the best model to predict suspended sediment used dimensions of road length times sloped squared, road surface type, and cutslope area. Using only precipitation and road dimensions, the best model to predict the peak flow of road runoff events used dimensions of road length times sloped squared and cutslope height. The cutslope height and cutslope area variables were found to be indicators of topographic positions that decreased hydrologic influences on the roads.

The combined measurement of runoff and suspended sediment load with the use of the Distributed Hydrology Soil Vegetation Model (DHSVM) present a method for interpreting impacts from the Phase III South Fork Caspar Creek 2017-2019 forest harvest, as well as different road scenarios and cumulative watershed effects for the watershed. Peak flows and suspended sediment loads were estimated to increase following forest harvest in the South Fork of Caspar Creek (417 ha) and the smaller Ziemer subwatershed (25 ha). The magnitude of peak flow increases were larger in the Ziemer subwatershed due to a greater proportion of forest harvested in the 2018 harvest, 75% basal area reduction compared to 42% for the South Fork of Caspar Creek. A modern road network placed on the upper slopes and ridges of the watershed, with few watercourse crossings, implemented with 2018 CFPRs, was demonstrated by DHSVM to be effective in reducing peak flow and suspended sediment inputs. Estimates of suspended sediment load and peak flows increased when different road drainage scenarios (e.g. pre-2010 CFPR, pre-1973 CFPR) with larger spacing between drainage structures were simulated.

The range of simulated suspended sediment load increase for South Fork Caspar Creek following the 2018 forest harvest was lower than the suspended sediment increase reported for the Phase II study of the North Fork of Caspar Creek six years following harvest. However, the high range of the suspended sediment did approach the North Fork Caspar Creek suspended sediment increases. The range of estimated suspended sediment load increase for the South Fork of Caspar was considerably higher when the pre-1974 road network, without benefit of modern CFPRs, was simulated. There was considerable uncertainty in the model performance and our assumptions regarding the pre-1974 road network. Nevertheless, the model comparisons between the legacy road network (designed for tractor-logging on steep slopes

with a high proportion of streamside roads and watercourse crossings) and the 2018 road network, were useful. The results indicate that hydrological disconnection of road networks, as required by the new CFPRs, will mitigate increases in peak flows and suspended sediment. However, even with hydrologic disconnection, a road network with a high proportion of streamside roads will continue to contribute to cumulative watershed effects.

Acknowledgements

This work was supported by funding from the California Department of Forestry and Fire Protection as part of the Caspar Creek Phase III experiment, Agreement #8CA03637. Pete Cafferata (Cal Fire) provided many useful comments and guidance to the success of this project. The USFS Pacific Southwest Research Station, Fort Bragg, provided the turbidity meters, Campbell Scientific data loggers, and pressure transducers. Supplemental data were provided by the Caspar Creek Experimental Watersheds project, which is funded by the USDA Forest Service Pacific Southwest Research Station and the California Department of Forestry and Fire Protection. Notably Elizabeth Keppeler and Jayme Seehafer provided considerable assistance with reviewing and providing Caspar Creek data sets used in the work. Samasoni Matagi provided support as the hydrologic technician for the data collection and corrections. Simon Marks provided time toward the statistical analysis and other data filtering tasks as needed. Julie Ridgeway compiled the meteorological data sets used in DHSVM and provided some limited field support. Andrew Adriance developed the UNIX cluster programs and scripts for the multi-run DHSVM Monte Carlo simulations. Tyler Davis and Simon Marks built the road flumes used for peak flow measurements; Tyler also participated in the pilot study. This work was further supported by the financial support of California Polytechnic State University during a faculty sabbatical.

LITERATURE CITED

Adriance, A. (2018). Optimizing the Distributed Hydrology Soil Vegetation Model for uncertainty assessment with serial, multicore and distributed accelerations. Master of Science thesis. California Polytechnic State University, San Luis Obispo, CA. 94 p.

Barrett, B., Kosaka, R., & Tomberlin, D. (2012). Road surface erosion on the Jackson Demonstration State Forest : results of a pilot study. In Standiford, R.B.; Weller, T.J.; Piirto, D. D.; Stuart, J.D, technical coordinators. Proceedings of coast redwood forests in a changing California: A symposium for scientists and managers. Gen. Tech. Rep. PSW-GTR-238. Albany, CA (pp. 13–21)

Berril, P. & O'Hara, K. 2007. Patterns of leaf area and growth efficiency in young even-aged and multiaged coast redwood stands. Canadian Journal of Forest Research, 37: 617-626. https://doi:10.1139/X06-271

Bowling, L. C., & Lettenmaier, D. P. (2001). The effects of forest roads and harvest on catchment hydrology in a mountainous maritime environment. In Land Use and Watersheds: Human Influence on Hydrology and Geomorphology in Urban and Forest Area. Water Science and Application Series Volume 2 (pp. 145–164). Washington, DC: American Geophysical Union. https://doi.org/10.1029/WS002p0145

Brown, K. R., Aust, W. M., & McGuire, K. J. (2013). Sediment delivery from bare and graveled forest road stream crossing approaches in the Virginia Piedmont. Forest ecology and management, 310, 836-846. https://doi.org/10.1016/j.foreco.2013.09.031

Burns, J.W. (1972). Some effects of logging and associated road construction on northern California streams. Transactions, American Fisheries Society 101(1): 1-17. https://www.fs.fed.us/psw/publications/4351/Burns72.pdf

Cafferata, P.H. (1989). Wet weather log hauling impacts on water quality. California Department of Forestry, Fort Bragg, CA. Jackson Demonstration State Forest Newsletter, No. 35, October 1989. p. 4-6.

Cafferata, P.H., & Reid L. M. (2013). Applications of long-term watershed research to forest management in California: 50 years of learning from the Caspar Creek Experimental Watersheds. California Forestry Report No. 5. State of California Department of Forestry and Fire Protection, Sacramento, CA. 110 p.

CAL FIRE (California Department of Forestry and Fire Protection). (2020). California Forest Practice Rules 2018. Title 14, California Code of Regulations, Resource Management, Forest Practice Program, Sacramento, CA, 408 p. Retrieved May, 2020 from: https://bof.fire.ca.gov/media/9478/2020-forest-practice-rules-and-act_final_ada.pdf

California Department of Water Resources (CDWR). (2019). The California Irrigation Management Information System. Retrieved January 2, 2019 from: https://wwwcimis.water.ca.gov/

Carr, A. E., Loague, K., & Vanderkwaak, J. E. (2014). Hydrologic-response simulations for the north fork of caspar creek: Second-growth, clear-cut, new-growth, and cumulative watershed effect scenarios. Hydrological Processes, 28(3), 1476–1494. https://doi.org/10.1002/hyp.9697

Coe, D. (2006). Sediment production and delivery from forest roads in the Sierra Nevada, California. Master of Science thesis, Colorado State University. Fort Collins, CO. 117 p.

Duan, Z. (2017). CreateStreamNetwork_PythonV. Retrieved February 8, 2019, from https://github.com/pnnl/DHSVM-PNNL/tree/master/CreateStreamNetwork_PythonV

Dymond, S. F. (2015). Caspar Creek experimental watersheds experiment three study plan: the influence of forest stand density reduction on watershed processes in the South Fork, 28 p. Retrieved Feb. 7, 2019 from: https://www.fs.fed.us/psw/topics/water/caspar/documents/CasparCreekStudyPlan.pdf

Dymond, S. F., Aust, W. M., Prisley, S. P., Eisenbies, M. H., & Vose, J. M. (2014). Application of a Distributed Process-Based Hydrologic Model to Estimate the Effects of Forest Road Density on Stormflows in the Southern Appalachians, 60 (December), 1213–1223.

Fu, B., Newham, L.T. and Ramos-Scharron, C.E. (2010). A review of surface erosion and sediment delivery models for unsealed roads. Environmental Modelling & Software, 25(1): 1-14.

Griffen, J. (2020). Personal communication on 1970s South Fork Caspar Creek road network, March 26, 2020. CAL FIRE Jackson Demonstration State Forest Retired Annuitant. Fort Bragg, CA.

Henry, N. (1998). Overview of the Caspar Creek Watershed Study. In Proceedings of the Conference on Coastal Watersheds: The Caspar Creek Story; R. Ziemer Tech. Ed. PSW-GTR-168 (pp. 1-9). Retrieved May, 2020 from: https://www.fs.fed.us/psw/publications/documents/psw_gtr168/psw_gtr168.pdf

Keppeler, E.T. (2019). Personal communication on soil auger holes for sub surface wells May 9, 2019. USDA Forest Service Pacific Southwest Research Station. Fort Bragg, CA.

Keppeler, E.T. (2012). Sediment production in a coastal watershed: legacy, land use, recovery, and rehabilitation. In: Standiford, R.B.; Weller, T.J.; Piirto, D.D.; Stuart, J.D., tech. coords. Proceedings of coast redwood forests in a changing California: A symposium for scientists and managers. Gen. Tech. Rep. PSW-GTR-238. Albany, CA: Pacific Southwest Research Station, Forest Service, U.S. Department of Agriculture. pp. 69-77. https://www.fs.fed.us/psw/publications/documents/psw_gtr238/psw_gtr238_069.pdf

Keppeler E., Brown, D. (1998). Subsurface drainage processes and management impacts. In Proceedings of the Conference on Coastal Watersheds: The Caspar Creek Story; R. Ziemer Tech. Ed. PSW-GTR-168 (pp. 1-9). Retrieved May, 2020 from: https://www.fs.fed.us/psw/publications/documents/psw_gtr168/psw_gtr168.pdf

Keppeler, E.T., P.H. Cafferata, and W.T. Baxter. (2007). State Forest Road 600: a riparian road decommissioning case study in Jackson Demonstration State Forest. California Forestry Note No. 120. California Department of Forestry and Fire Protection. Sacramento, CA. 22 p. http://www.fs.fed.us/psw/topics/water/caspar/pubs/Rd600DecomNote.pdf

Krause, P., Boyle, D.P., & Bäse, F. (2005). Comparison of different efficiency criteria for hydrologic model assessment. Adv. Geosci. 5, 89–97.

Lewis, J. (1998). Evaluating the impacts of logging activities on erosion and suspended sediment transport in the Caspar Creek watersheds. In Proceedings of the Conference on Coastal Watersheds: The Caspar Creek Story; R. Ziemer Tech. Ed. PSW-GTR-168 (pp. 1-9). Retrieved May, 2020 from: https://www.fs.fed.us/psw/publications/documents/psw_gtr168/psw_gtr168.pdf

Lewis, J.; Eads, R.E. (2009). Implementation guide for turbidity threshold sampling: principles, procedures, and analysis. Gen. Tech. Rep. PSW-GTR-212. Albany, CA: U.S. Department of Agriculture, Forest Service, Pacific Southwest Research Station. 86 p. https://www.fs.fed.us/psw/publications/4351/Lewis2009.pdf

Lewis, J., Mori, S., Keppeler, E., & Ziemer, R. (2001). Impacts of logging on stream peak flows, flow volumes and suspended sediment loads in Caspar Creek, California. In: Wigmosta, M. Burges, S. (ed.) Land Use and Watersheds: Human Influence on Hydrology and Geomorphology in Urban and Forest Areas. Water Science and Application, Vol. 2, American Geophysical Union, Washington, D.C., 85-125.

Luce, C. (2002). Hydrological processes and pathways affected by forest roads: what do we still need to learn? Hydrol. Process. 16, 2901–2904

Luce, C. H., Black, T. A. (1999). Sediment production from forest roads in western Oregon. Water Resources Research 35: 2561-2570.

Megahan, W. and W. Kidd. (1972). Effects of logging and logginf roads on erosion and sediment deposition from steep terrain. Journal of Forestry, March Issue, 136-141

Oregon Forest Resources Institute. (2011). Oregon's forest protection laws, revised, second edition. Oregon Forest Resources Institute, Portland, OR. 196 p.

Reid, L.M. (2012). Comparing hydrologic responses to tractor-yarded selection and cable-yarded clearcut logging in a coast redwood forest. In: Standiford, R.B.; Weller, T.J.; Piirto, D.D.; Stuart, J.D., (Technical Coordinators). Proceedings of coast redwood forests in a changing California: A symposium for scientists and managers. General Technical Report PSW-GTR-238. Albany, CA: U.S. Department of Agriculture, Forest Service, Pacific Southwest Research Station: 151-161.

Reid, L.M.; Dewey, N.J.; Lisle, T.E.; Hilton, S.J. (2010). The incidence and role of gullies after logging in a coastal redwood forest. Geomorphology. 117: 115-169.

Reid, L. and Dunne, T. (1984). Sediment production from forest roads. Water Resources Research, Vol. 20, No. 11, 1753-1761

Reid, L. M.; Lewis, J. (2009). Rates, timing, and mechanisms of rainfall interception loss in a coastal redwood forest. Journal of Hydrology. 375: 459-470.

Rice, R., Tilley, F.B., & Datzman, P. A. (1979). A watershed's response to logging and roads: South Fork of Caspar Creek, California, 1967-1976. Research Paper PSW-146. USDA Forest Service, Pacific Southwest Forest and Range Experiment Station, Berkeley, CA., 12.

Ridgeway, J. (2019). An analysis of changes in stream temperature due to forest harvest practices using DHSVM-RBM. Master of Science thesis. California Polytechnic State University. San Luis Obispo, CA. 116 p. https://digitalcommons.calpoly.edu/cgi/viewcontent.cgi?article=3450&context=theses

Ritter A, & Muñoz-Carpena R. (2013). Performance evaluation of hydrological models : Statistical significance for reducing subjectivity in goodness-of-fit assessments. J Hydrol.480: 33–45. http://dx.doi.org/10.1016/j.jhydrol.2012.12.004

Rittiman, C. A. and T. Thorson. (2006). Soil Survey of Mendocino County, California, Western Part. USDA Natural Resources Conservation Service. 456 p.

Samani, Z., and Herrera, E. 1996. A low-cost water measuring device. New Mexico State University Cooperative Extension, Guide M-226; PH-4-205. 4 p.

Storck, P., Bowling, L., Wetherbee, P., and Lettenmaier, D. (1998). Application of a GIS-based distributed hydrology model for prediction of forest harvest effects on peak stream flow in the Pacific Northwest. Hydrological Processes, 12(6), 889–904.

Storck, P., Lettenmaier, D., Connelly, B.A., and Cundy, T. W. (1995). Implications of forest practices on downstream flooding: phase II final report. Washington Forest Practices Association, Olympia, WA. 100 p.

Surfleet, C. G., Skaugset III, A. E., & McDonnell, J. J. (2010). Uncertainty assessment of forest road modeling with the Distributed Hydrology Soil Vegetation Model (DHSVM). Canadian Journal of Forest Research, 40, 1397–2010. https://doi.org/10.1139/X10-079

Surfleet, C. G., Skaugset III, A. E., & Meadows, M. W. (2011). Road runoff and sediment sampling for determining road sediment yield at the watershed scale. Canadian Journal of Forest Research, 41(10), 1970–1980. https://doi.org/10.1139/x11-104

Surfleet, C., Tullos**,** D. **(**2012**)**. Uncertainty assessment of hydrologic response to climate change for the Santiam River, Oregon. Hydrologic Processes, DOI: 10.1002/hyp.9485, 16 p.

Wagenbrenner, J. (2018). Addendum to Caspar Creek Experimental Watersheds Experiment Three Study Plan: The influence of forest stand density reduction on watershed processes in the South Fork. Tech. rep., USDA Forest Service Pacific Southwest Research Station

Weaver, W.E., Weppner, E.M. and Hagans, D.K. (2015). Handbook for forest, ranch and rural roads: a guide for planning, designing, constructing, reconstructing, upgrading, maintaining and closing wildland roads (Rev. 1st ed.). Mendocino County Resource Conservation District, Ukiah, CA. 341 p. plux appendices. Retrieved May, 2020 from: http://www.pacificwatershed.com/sites/default/files/roadsenglishbookapril2015b_0.pdf

Webb, L. (2019; 2020). Unpublished forest stand data from Jackson Demonstration State Forest. April, 2019. May, 2020. Fort Bragg, CA.
Wemple B., Jones J., Grant G. (1996). Channel network extension by logging roads in two basins, western Cascades, Oregon. Water Resources Bulletin 32: 1195–1207.

Wigmosta M.S., Perkins, W. A. (2001). Simulating the effects of forest roads on watershed hydrology. Land Use and Watersheds: Human Influence on Hydrology and Geomorphology in Urban and Forest Areas, 127–143.

Wigmosta, M. S., Vail, L. W., & Lettenmaier, D. P. (1994). A distributed hydrology-vegetation model for complex terrain. Water Resources Research. https://doi.org/10.1029/94WR00436

Yearsley J. (2012). A grid-based approach for simulating stream temperature. Wat. Resour. Res., 48. http://dx.doi.org/10.1029/2011WR011515.

Yearsley J. (2009). A semi-Lagrangian water temperature model for advection-dominated river systems, Water Resour. Res, http://dx.doi.org/doi:10.1029/2008WR007629.

Ziemer, R.R. (1992). Effect of logging on pipeflow and erosion, coastal northern California, USA In: Walling, D.E.; Davies, T.R.; Hasholt, B., eds. Erosion, debris flows and environment in mountain regions, proceedings of the Chendu symposium; 1992 July 5-9; Chendu, China. International Association of Hydrological Sciences Publication No. 209. 187-197.

Ziemer, R.R. (Technical Coordinator). (1998a). Proceedings of the Conference on Coastal Watersheds: the Caspar Creek Story, May 6, 1998; Ukiah, CA. General Tech. Rep. PSW GTR-168. Albany, CA: U.S. Department of Agriculture, Forest Service, Pacific Southwest Research Station. 149 p. https://www.fs.fed.us/psw/publications/documents/psw_gtr168/

Ziemer, R. R. (1998b). Flooding and storms. In Proceedings of the Conference on Coastal Watersheds: The Caspar Creek Story; R. Ziemer Tech. Ed. PSW-GTR-168 (pp. 15–24). Retrieved Feb. 6, 2019 from: https://www.fs.fed.us/psw/publications/documents/psw_gtr168/psw_gtr168.pdf